Minnesota Department of Transportation

RESEARCH SERVICES

Office of Policy Analysis, Research & Innovation

Air Voids Testing for MnROAD Cells

Mihai Marasteanu, Principal Investigator
Department of Civil Engineering
University of Minnesota

July 2010

Research Project
Final Report 2010-28

Your Destination...Our Priority

Technical Report Documentation Page

1. Report No.	2.	3. Recipients Accession No.
MN/RC 2010-28		

4. Title and Subtitle	5. Report Date
Air Voids Testing for MnROAD Cells	July 2010
	6.

7. Author(s)	8. Performing Organization Report No.
Mugurel Turos, Ki Hoon Moon, Mihai Marasteanu	

9. Performing Organization Name and Address	10. Project/Task/Work Unit No.
Department of Civil Engineering University of Minnesota 500 Pillsbury Dr. SE Minneapolis, Minnesota 55455	CTS Project #2010040
	11. Contract (C) or Grant (G) No. (c) 89261 (wo) 171

12. Sponsoring Organization Name and Address	13. Type of Report and Period Covered
Minnesota Department of Transportation Research Services Section 395 John Ireland Boulevard, Mail Stop 330 St. Paul, Minnesota 55155-1899	Final Report
	14. Sponsoring Agency Code

15. Supplementary Notes
http://www.lrrb.org/pdf/201028.pdf

16. Abstract (Limit: 250 words)

This report summarizes the experimental work performed on cores extracted from various cells at MnROAD to determine the air void content of the different asphalt mixtures used in these cells. Analysis of the data was not part of this study.

17. Document Analysis/Descriptors	18. Availability Statement
Hot mix paving mixtures, Air voids, Corelock, Voids in mineral aggregate (VMA), Digital imaging, MnROAD	No restrictions. Document available from: National Technical Information Services, Springfield, Virginia 22161

19. Security Class (this report)	20. Security Class (this page)	21. No. of Pages	22. Price
Unclassified	Unclassified	52	

Air Voids Testing for MnROAD Cells

Final Report

Prepared by:

Mugurel Turos
Ki Hoon Moon
Mihai Marasteanu

Department of Civil Engineering
University of Minnesota

July 2010

Published by:

Minnesota Department of Transportation
Research Services Section
395 John Ireland Boulevard, MS 330
St. Paul, Minnesota 55155-1899

TABLE OF CONTENTS

LIST OF TABLES

LIST OF FIGURES

EXECUTIVE SUMMARY

MnROAD has undergone a large-scale reconstruction project during the summer of 2008. Several of the test sections were surfaced with hot mix asphalt. The material properties measured in the lab are expected to give an indication of the pavement performance in the field. One of the most important pieces of information is the amount, or percent, of air voids in the mixtures. In this project, experimental work was performed to measure air voids in the lifts of 145 cores extracted from various cells at MnROAD. Analysis of the results was not part of this study.

INTRODUCTION

MnROAD has undergone a large-scale reconstruction project during the summer of 2008. Several of the test sections were surfaced with hot mix asphalt. In order to support current and future research efforts, it is critically important to obtain relevant properties of pavement materials starting from the construction process to the end of the service life of the pavements. One of the most important properties is the percent of air voids in the mixtures. In this project, cores extracted from various cells at MnROAD were used to determine the air void content of the different asphalt mixtures used in these cells.

LABORATORY SAMPLE PREPARATION

A total of 342 mixture samples from 145 field cores extracted from various cells at MnROAD were received in the Pavement Laboratory at University of Minnesota. A description of the cores is provided in Table 1.

Air voids were determined according to AASHTO T166 for each lift of each core, and an average was calculated if two replicates were available. The results will be used by researchers at MnDOT to compare air voids in the Outer Wheel Path vs. Between Wheel Path, Driving vs. Passing, Inside vs. Outside Lane, and Longitudinal Joint where applicable

The following procedure was used to perform the measurements:

- First, the separation plan between the different lifts was highlighted for each core using a marker.
- An Excel table was prepared, and each layer of each core of each cell received a unique identification number. That number was written on the correspondent core/layer. A paper plate was also labeled with the identification number and the sample's name, see Figure 1.
- The cores were then cut and each sample was placed on a separate paper plate and stored to dry before testing, see Figure 2. Before testing was performed, each sample was scanned on both faces for digital imaging processing.
- The Novachip lift from Cells 2 and 3 was tested using the Corelock device at Mn/DOT.
- The bottom layer for Cells 2, 3, and 4, emulsion stabilized FDR, was first tested using Method A from the standard and then sent to Mn/DOT for Corelock testing.

Figure 1. Identifying cores used in air voids determination

Table 1. MnROAD cores identification

				Driving/Inside Lane		Passing/Outside Lane		Long Jt		
Cell	Lift	Thickness	Description	OWP Cores	BWP Cores	OWP Cores	BWP Cores	Cores	Total Cores	Total Specimens
1	3	1.5	52-34 inlay (DL)	1	1	0	0		2	2
2	1	6	EE stabilized FDR	2	2	2	2		8	24
	2	2	Superpave							
	3	0.75	Novachip							
3	1	6	EE stabilized FDR	2	2	2	2		8	24
	2	2	Superpave							
	3	0.75	Novachip							
4	1	8	EE stabilized FDR	1	1	1	1		4	12
	2	2	Superpave							
	3	1	Superpave							
6	1	2	4.75 mm taconite	1	1	1	1		4	4
15	1	1.5	WMA wear	1	1	1	1		8	16
	2	1.5	WMA wear							
16	1	2	WMA non wear	1	1	1	1	1	5	15
	2	1.5	WMA wear							
	3	1.5	WMA wear							
17	1	2	WMA non wear	1	1	1	1		4	12
	2	1.5	WMA wear							
	3	1.5	WMA wear							
18	1	2	WMA non wear	1	1	1	1		4	12
	2	1.5	WMA wear							
	3	1.5	WMA wear							
19	1	2	WMA non wear	2	2	2	2	1	9	27
	2	1.5	WMA wear							
	3	1.5	WMA wear							
20	1	2	FRAP non wear	2	2	2	2		8	24
	2	1.5	FRAP wear							
	3	1.5	FRAP wear							
21	1	2	FRAP non wear	2	2	2	2		8	24
	2	1.5	FRAP wear							
	3	1.5	FRAP wear							
22	1	2	FRAP non wear	2	2	2	2		8	24
	2	1.5	FRAP wear							
	3	1.5	FRAP wear							
23	1	2	WMA non wear	1	1	1	1		4	12
	2	1.5	WMA wear							
	3	1.5	WMA wear							
19	1	1.5	TO wear	0	2	0	0	1	3	6
shld	2	1.5	TO wear							
5	1	1.5	MW wear	0	2	0	0	1	3	6
shld	2	1.5	MW wear							
24	1	1.5	HMA wear	1	1	1	1	1	5	10
	2	1.5	HMA wear							
86	1	5	porous	2	2	1	1		6	6
88	1	5	porous	2	2	1	1		6	6
77	1	2	PPA + Elvaloy	1	1	1	1		4	8
	2	2	PPA + Elvaloy							
78	1	2	PPA + Elvaloy	2	2	1	1		6	12
	2	2	PPA + Elvaloy							
79	1	2	PPA + Elvaloy	1	1	1	1		4	8
	2	2	PPA + Elvaloy							
31	1	2	taconite HMA	1	1	1	1		4	8
	2	2	taconite HMA							
33	1	2	PPA	2	2	1	1		6	12
	2	2	PPA							
34	1	2	PPA + SBS	2	2	1	1	1	7	14
	2	2	PPA + SBS							
35	1	2	SBS	2	2	1	1	1	7	14
	2	2	SBS							

Figure 2. Storing samples used in air voids determination

- All the other samples were tested in the lab using both methods A and C in AASHTO T 166-05, as described below:

Method A

The following values were recorded:
A= mass in grams of the specimen in air
B= mass in grams of the surface-dry specimen in air
C= mass in grams of the specimen in water

Bulk specific gravity, Gmb was calculated as $= \frac{A}{B-C}$

Method C

The specimen was placed in a large flat bottom pan of known mass (Figure 3) and then kept in an oven at 110 C until it was possible to separate the sample in fine particles (Figure 4). The pan was placed back in the oven and dried to a constant mass. The pan and the specimen were cooled down to room temperature and the dry mass A was recorded. Bulk specific gravity was calculated using the same equation as above.
The maximum specific gravity (Gmm) values for each cell/core/layer were obtained at Mn/DOT.

The air void content (AV) was calculated as $= 1 - \frac{Gmb}{Gmm}$

Figure 3. Flat bottom pan used in air voids determination

Figure 4. Broken down mixtures used in air voids determination

TEST RESULTS

The air void results obtained from performing the test methods described above are tabulated in Tables 2 to 8. Note that the following identification was used for lifts within the same core:

- A: top lift
- B: intermediate lift
- C: bottom lift

Plots of the results using Method A are shown in Figures 5 to 30. For cells 2, and 3, Corelock results were used for the top lift. For cells 86 and 88, only Corelock results were available.

Table 2. Test results for Cells 1, 2, and 3

Cell	Core	Location	Lift	Bulk specific gravity			Gmm	Air voids,%		
				Method A	Method C	Corelok		Method A	Method C	Corelok
1	1	DL-OWP	3A	2.397	2.390		2.476	3.2	3.5	
	2	DL-BWP	3A	2.370	2.361		2.476	4.3	4.6	
2	1	DL-OWP	1C	2.294			2.439	5.9		
			2B	2.362	2.353		2.496	5.4	5.7	
			3A			2.173	2.467			10.9
	2	DL-OWP	1C	2.284		2.278	2.439	6.4		6.6
			2B	2.365	2.358		2.496	5.2	5.5	
			3A			2.168	2.467			12.5
	3	DL-BWP	1C	2.274		2.268	2.439	6.8		7.0
			2B	2.374	2.367		2.496	4.9	5.2	
			3A			2.161	2.467			12.8
	4	DL-BWP	1C*	2.224			2.439	8.8		
			2B	2.362	2.356		2.496	5.4	5.6	
			3A			2.157	2.467			13.0
	5	PL-OWP	1C	2.257		2.249	2.439	7.5		7.8
			2B	2.407	2.402		2.496	3.6	3.8	
			3A			2.190	2.467			11.7
	6	PL-OWP	1C	2.283		2.280	2.439	6.4		6.5
			2B	2.397	2.392		2.496	4.0	4.2	
			3A			2.186	2.467			11.8
	7	PL-BWP	1C	2.279		2.274	2.439	6.6		6.8
			2B	2.344	2.339		2.496	6.1	6.3	
			3A			2.135	2.467			13.9
	8	PL-BWP	1C	2.269		2.264	2.439	7.0		7.2
			2B	2.337	2.331		2.496	6.4	6.6	
			3A			2.150	2.467			13.3
3	1	DL-OWP	1C	2.212		2.206	2.450	9.7		10.0
			2B	2.359	2.350		2.496	5.5	5.8	
			3A			2.143	2.467			12.5
	2	DL-OWP	1C	2.237		2.231	2.450	8.7		9.0
			2B	2.353	2.344		2.496	5.7	6.1	
			3A			2.147	2.467			13.4
	3	DL-BWP	1C	2.224		2.225	2.450	9.2		9.2
			2B	2.354	2.347		2.496	5.7	6.0	
			3A			2.187	2.467			11.8
	4	DL-BWP	1C	2.249		2.245	2.450	8.2		8.4
			2B	2.373	2.363		2.496	4.9	5.3	
			3A			2.189	2.467			11.7
	5	PL-OWP	1C	2.248	2.238		2.450	8.2	8.7	
			2B	2.408	2.402		2.496	3.5	3.8	
			3A			2.109	2.467			14.9
	6	PL-OWP	1C	2.286		2.278	2.450	6.7		7.0
			2B	2.419	2.414		2.496	3.1	3.3	
			3A			2.124	2.467			14.4
	7	PL-BWP	1C	2.230		2.222	2.450	9.0		9.3
			2B	2.358	2.350		2.496	5.5	5.9	
			3A			2.116	2.467			14.7
	8	PL-BWP	1C	2.252	2.242		2.450	8.1	8.5	
			2B	2.368	2.360		2.496	5.1	5.5	
			3A			2.084	2.467			16.0

Table 3. Test results for Cells 4, 5, 6, 15, and 16

Cell	Core	Location	Lift	Bulk specific gravity			Gmm	Air voids,%		
				Method A	Method C	Corelok		Method A	Method C	Corelok
4	1	DL-OWP	1C	2.375		2.381	2.489	4.6		4.3
			2B	2.336	2.325		2.496	6.4	6.8	
			3A	2.339	2.330		2.496	6.3	6.6	
	2	DL-BWP	1C	2.358		2.263	2.489	5.3		5.1
			2B	2.331	2.322		2.496	6.6	7.0	
			3A	2.349	2.341		2.496	5.9	6.2	
	3	PL-OWP	1C	2.385		2.392	2.489	4.2		3.9
			2B	2.377	2.371		2.496	4.8	5.0	
			3A	2.353	2.344		2.496	5.7	6.1	
	4	PL-BWP	1C	2.386		2.388	2.489	4.1		4.1
			2B	2.378	2.370		2.496	4.7	5.0	
			3A	2.317	2.308		2.496	7.2	7.5	
5	1	shld-mat	1B	2.292	2.287		2.527	9.3	9.5	
			2A	2.254	2.249		2.527	10.8	11.0	
	2	shld-mat	1B	2.327	2.320		2.527	7.9	8.2	
			2A	2.283	2.277		2.527	9.6	9.9	
	3	shld-LJT	1B	2.258	2.253		2.527	10.7	10.9	
			2A	2.235	2.230		2.527	11.5	11.8	
6	10	DL-OWP	1A	2.422	2.414		2.543	4.8	5.1	
	11	DL-BWP	1A	2.349	2.340		2.543	7.6	8.0	
	12	PL-OWP	1A	2.375	2.361		2.543	6.6	7.2	
	13	PL-BWP	1A	2.340	2.327		2.543	8.0	8.5	
15	1	DL-OWP	1B	2.369	2.361		2.509	5.6	5.9	
			2A	2.410	2.398		2.509	4.0	4.4	
	2	DL-BWP	1B	2.339	2.327		2.509	6.8	7.3	
			2A	2.298	2.285		2.509	8.4	8.9	
	3	PL-OWP	1B	2.334	2.320		2.509	7.0	7.5	
			2A	2.363	2.351		2.509	5.8	6.3	
	4	PL-BWP	1B	2.325	2.314		2.509	7.4	7.8	
			2A	2.358	2.350		2.509	6.0	6.3	
16	1	DL-OWP	1C	2.397	2.391		2.483	3.5	3.7	
			2B	2.357	2.349		2.509	6.0	6.4	
			3A	2.358	2.345		2.509	6.0	6.5	
	2	DL-BWP	1C	2.387	2.380		2.483	3.9	4.2	
			2B	2.300	2.286		2.509	8.3	8.9	
			3A	2.303	2.294		2.509	8.2	8.6	
	3	PL-OWP	1C	2.379	2.370		2.483	4.2	4.6	
			2B	2.344	2.333		2.509	6.6	7.0	
			3A	2.371	2.359		2.509	5.5	6.0	
	4	PL-BWP	1C	2.392	2.388		2.483	3.7	3.8	
			2B	2.336	2.325		2.509	6.9	7.3	
			3A	2.302	2.295		2.509	8.3	8.5	
	5	DL-CJT	1C	2.290	2.284		2.483	7.8	8.0	
			2B	2.308	2.297		2.509	8.0	8.4	
			3A	2.261	2.251		2.509	9.9	10.3	

Table 4. Test results for Cells 17, 18, and 19

Cell	Core	Location	Lift	Bulk specific gravity			Gmm	Air voids,%		
				Method A	Method C	Corelok		Method A	Method C	Corelok
17	1	DL-OWP	1C	2.366	2.356		2.483	4.7	5.1	
			2B	2.372	2.360		2.509	5.4	5.9	
			3A	2.375	2.365		2.509	5.4	5.8	
	2	DL-BWP	1C	2.350	2.342		2.483	5.3	5.7	
			2B	2.304	2.289		2.509	8.2	8.8	
			3A	2.318	2.305		2.509	7.6	8.1	
	3	PL-OWP	1C	2.388	2.377		2.483	3.8	4.3	
			2B	2.299	2.278		2.509	8.4	9.2	
			3A	2.318	2.303		2.509	7.6	8.2	
	4	PL-BWP	1C	2.381	2.376		2.483	4.1	4.3	
			2B	2.303	2.290		2.509	8.2	8.7	
			3A	2.292	2.282		2.509	8.7	9.0	
18	1	DL-OWP	1C	2.398	2.392		2.483	3.4	3.7	
			2B	2.384	2.378		2.509	5.0	5.2	
			3A	2.406	2.394		2.509	4.1	4.6	
	2	DL-BWP	1C	2.395	2.389		2.483	3.5	3.8	
			2B	2.303	2.292		2.509	8.2	8.7	
			3A	2.321	2.314		2.509	7.5	7.8	
	3	PL-OWP	1C	2.361	2.356		2.483	4.9	5.1	
			2B	2.274	2.262		2.509	9.4	9.8	
			3A	2.325	2.318		2.509	7.3	7.6	
	4	PL-BWP	1C	2.357	2.348		2.483	5.1	5.4	
			2B	2.322	2.312		2.509	7.4	7.9	
			3A	2.371	2.360		2.509	5.5	5.9	
19	1	DL-OWP	1C	2.381	2.376		2.483	4.1	4.3	
			2B	2.409	2.399		2.509	4.0	4.4	
			3A	2.396	2.385		2.509	4.5	4.9	
	2	DL-OWP	1C	2.343	2.335		2.483	5.6	5.9	
			2B	2.395	2.385		2.509	4.6	5.0	
			3A	2.406	2.397		2.509	4.1	4.5	
	3	DL-BWP	1C	2.311	2.305		2.483	6.9	7.2	
			2B	2.381	2.372		2.509	5.1	5.5	
			3A	2.372	2.364		2.509	5.5	5.8	
	4	DL-BWP	1C	2.336	2.329		2.483	5.9	6.2	
			2B	2.384	2.378		2.509	5.0	5.2	
			3A	2.356	2.349		2.509	6.1	6.4	
	5	PL-OWP	1C	2.419	2.412		2.483	2.6	2.9	
			2B	2.288	2.278		2.509	8.8	9.2	
			3A	2.277	2.262		2.509	9.2	9.9	
	6	PL-OWP	1C	2.405	2.397		2.483	3.1	3.5	
			2B	2.250	2.241		2.509	10.3	10.7	
			3A	2.279	2.267		2.509	9.2	9.6	
	7	PL-BWP	1C	2.391	2.383		2.483	3.7	4.0	
			2B	2.298	2.289		2.509	8.4	8.8	
			3A	2.257	2.248		2.509	10.1	10.4	
	8	PL-BWP	1C	2.388	2.379		2.483	3.8	4.2	
			2B	2.318	2.310		2.509	7.6	7.9	
			3A	2.258	2.248		2.509	10.0	10.4	
	9	DL-CJT	1C	2.292	2.285		2.483	7.7	8.0	
			2B	2.320	2.310		2.509	7.5	7.9	
			3A	2.347	2.338		2.509	6.5	6.8	

Table 5. Test results for Cells 19s, 20, and 21

Cell	Core	Location	Lift	Bulk specific gravity			Gmm	Air voids,%		
				Method A	Method C	Corelok		Method A	Method C	Corelok
19s	10	shld-mat	1B	2.378	2.374		2.547	6.6	6.8	
			2A	2.263	2.260		2.547	11.1	11.3	
	11	shld-mat	1B	2.379	2.374		2.547	6.6	6.8	
			2A	2.261	2.257		2.547	11.2	11.4	
	12	shld-mat	1B	2.344	2.336		2.547	8.0	8.3	
			2A	2.252	2.248		2.547	11.6	11.7	
20	1	DL-OWP	1C	2.333	2.324		2.476	5.8	6.1	
			2B	2.381	2.372		2.527	5.8	6.1	
			3A	2.393	2.384		2.527	5.3	5.7	
	2	DL-OWP	1C	2.335	2.326		2.476	5.7	6.1	
			2B	2.387	2.380		2.527	5.5	5.8	
			3A	2.369	2.361		2.527	6.3	6.6	
	3	DL-BWP	1C	2.364	2.360		2.476	4.5	4.7	
			2B	2.358	2.350		2.527	6.7	7.0	
			3A	2.357	2.352		2.527	6.7	6.9	
	4	DL-BWP	1C	2.359	2.356		2.476	4.7	4.9	
			2B	2.368	2.360		2.527	6.3	6.6	
			3A	2.355	2.349		2.527	6.8	7.0	
	5	PL-OWP	1C	2.356	2.348		2.476	4.9	5.2	
			2B	2.397	2.394		2.527	5.1	5.3	
			3A	2.349	2.344		2.527	7.0	7.2	
	6	PL-OWP	1C	2.361	2.355		2.476	4.7	4.9	
			2B	2.425	2.421		2.527	4.1	4.2	
			3A	2.365	2.359		2.527	6.4	6.7	
	7	PL-BWP	1C	2.370	2.367		2.476	4.3	4.4	
			2B	2.384	2.379		2.527	5.7	5.9	
			3A	2.350	2.343		2.527	7.0	7.3	
	8	PL-BWP	1C	2.374	2.371		2.476	4.1	4.2	
			2B	2.399	2.395		2.527	5.1	5.2	
			3A	2.364	2.357		2.527	6.5	6.7	
21	1	DL-OWP	1C	2.381	2.373		2.477	3.9	4.2	
			2B	2.425	2.422		2.507	3.3	3.4	
			3A	2.395	2.388		2.507	4.5	4.8	
	2	DL-OWP	1C	2.375	2.369		2.477	4.1	4.4	
			2B	2.423	2.421		2.507	3.4	3.4	
			3A	2.400	2.392		2.507	4.3	4.6	
	3	DL-BWP	1C	2.363	2.358		2.477	4.6	4.8	
			2B	2.393	2.386		2.507	4.6	4.8	
			3A	2.346	2.340		2.507	6.4	6.7	
	4	DL-BWP	1C	2.380	2.376		2.477	3.9	4.1	
			2B	2.387	2.379		2.507	4.8	5.1	
			3A	2.345	2.339		2.507	6.5	6.7	
	5	PL-OWP	1C	2.391	2.388		2.477	3.5	3.6	
			2B	2.433	2.431		2.507	3.0	3.0	
			3A	2.391	2.383		2.507	4.6	4.9	
	6	PL-OWP	1C	2.382	2.377		2.477	3.8	4.0	
			2B	2.440	2.437		2.507	2.7	2.8	
			3A	2.402	2.394		2.507	4.2	4.5	
	7	PL-BWP	1C	2.404	2.401		2.477	2.9	3.1	
			2B	2.408	2.404		2.507	4.0	4.1	
			3A	2.370	2.364		2.507	5.5	5.7	
	8	PL-BWP	1C	2.391	2.387		2.477	3.5	3.6	
			2B	2.386	2.382		2.507	4.8	5.0	
			3A	2.372	2.368		2.507	5.4	5.5	

Table 6. Test results for Cells 22, 23, and 24

Cell	Core	Location	Lift	Bulk specific gravity			Gmm	Air voids,%		
				Method A	Method C	Corelok		Method A	Method C	Corelok
22	1	DL-OWP	1C	2.379	2.374		2.473	3.8	4.0	
			2B	2.391	2.384		2.504	4.5	4.8	
			3A	2.371	2.363		2.504	5.3	5.6	
	2	DL-OWP	1C	2.369	2.363		2.473	4.2	4.4	
			2B	2.379	2.373		2.504	5.0	5.2	
			3A	2.380	2.368		2.504	5.0	5.4	
	3	DL-BWP	1C	2.351	2.344		2.473	5.0	5.2	
			2B	2.380	2.371		2.504	5.0	5.3	
			3A	2.321	2.311		2.504	7.3	7.7	
	4	DL-BWP	1C	2.367	2.361		2.473	4.3	4.5	
			2B	2.349	2.341		2.504	6.2	6.5	
			3A	2.343	2.334		2.504	6.4	6.8	
	5	PL-OWP	1C	2.394	2.389		2.473	3.2	3.4	
			2B	2.363	2.357		2.504	5.6	5.9	
			3A	2.348	2.338		2.504	6.2	6.6	
	6	PL-OWP	1C	2.392	2.387		2.473	3.3	3.5	
			2B	2.379	2.372		2.504	5.0	5.3	
			3A	2.353	2.344		2.504	6.0	6.4	
	7	PL-BWP	1C	2.378	2.374		2.473	3.8	4.0	
			2B	2.399	2.393		2.504	4.2	4.4	
			3A	2.382	2.376		2.504	4.9	5.1	
	8	PL-BWP	1C	2.392	2.388		2.473	3.3	3.4	
			2B	2.381	2.375		2.504	4.9	5.2	
			3A	2.374	2.369		2.504	5.2	5.4	
23	1	DL-OWP	1C	2.363	2.358		2.483	4.8	5.0	
			2B	2.350	2.340		2.509	6.3	6.7	
			3A	2.382	2.374		2.509	5.1	5.4	
	2	DL-BWP	1C	2.363	2.358		2.483	4.8	5.0	
			2B	2.323	2.314		2.509	7.4	7.8	
			3A	2.325	2.316		2.509	7.3	7.7	
	3	PL-OWP	1C	2.387	2.383		2.483	3.9	4.0	
			2B	2.327	2.319		2.509	7.3	7.6	
			3A	2.319	2.312		2.509	7.6	7.9	
	4	PL-BWP	1C	2.412	2.408		2.483	2.9	3.0	
			2B	2.354	2.348		2.509	6.2	6.4	
			3A	2.362	2.356		2.509	5.9	6.1	
24	9	IL-OWP	1B	2.380	2.375		2.504	5.0	5.2	
			2A	2.378	2.374		2.504	5.0	5.2	
	10	IL-BWP	1B	2.378	2.374		2.504	5.0	5.2	
			2A	2.358	2.353		2.504	5.8	6.0	
	11	OL-OWP	1B	2.396	2.392		2.504	4.3	4.5	
			2A	2.324	2.318		2.504	7.2	7.4	
	12	OL-BWP	1B	2.368	2.362		2.504	5.4	5.7	
			2A	2.272	2.267		2.504	9.3	9.5	
	13	OL-CLJT	1B	2.298	2.289		2.504	8.2	8.6	
			2A	2.315	2.311		2.504	7.5	7.7	

Table 7. Test results for Cells 31, 33, 34, and 35

Cell	Core	Location	Lift	Bulk specific gravity			Gmm	Air voids,%		
				Method A	Method C	Corelok		Method A	Method C	Corelok
31	1	IL-OWP	1B	2.570	2.565		2.659	3.4	3.6	
			2A	2.525	2.519		2.659	5.0	5.3	
	2	IL-BWP	1B	2.583	2.578		2.659	2.8	3.0	
			2A	2.504	2.497		2.659	5.8	6.1	
	3	OL-OWP	1B	2.551	2.542		2.659	4.1	4.4	
			2A	2.536	2.523		2.659	4.6	5.1	
	4	OL-BWP	1B	2.545	2.536		2.659	4.3	4.6	
			2A	2.559	2.552		2.659	3.8	4.0	
33	1	IL-OWP	1B	2.387	2.383		2.478	3.7	3.9	
			2A	2.370	2.364		2.478	4.4	4.6	
	2	IL-OWP	1B	2.392	2.387		2.478	3.5	3.7	
			2A	2.387	2.382		2.478	3.7	3.9	
	3	IL-BWP	1B	2.356	2.352		2.478	4.9	5.1	
			2A	2.334	2.329		2.478	5.8	6.0	
	4	IL-BWP	1B	2.357	2.351		2.478	4.9	5.1	
			2A	2.338	2.332		2.478	5.6	5.9	
	5	OL-OWP	1B	2.410	2.406		2.478	2.7	2.9	
			2A	2.341	2.336		2.478	5.5	5.7	
	6	OL-BWP	1B	2.359	2.349		2.478	4.8	5.2	
			2A	2.297	2.290		2.478	7.3	7.6	
34	1	IL-OWP	1B	2.354	2.347		2.474	4.9	5.1	
			2A	2.373	2.368		2.474	4.1	4.3	
	2	IL-OWP	1B	2.354	2.345		2.474	4.9	5.2	
			2A	2.367	2.363		2.474	4.3	4.5	
	3	IL-BWP	1B	2.320	2.307		2.474	6.2	6.8	
			2A	2.334	2.327		2.474	5.7	5.9	
	4	IL-BWP	1B	2.327	2.314		2.474	5.9	6.5	
			2A	2.333	2.326		2.474	5.7	6.0	
	5	OL-OWP	1B	2.373	2.369		2.474	4.1	4.2	
			2A	2.377	2.370		2.474	3.9	4.2	
	6	OL-BWP	1B	2.335	2.329		2.474	5.6	5.9	
			2A	2.309	2.301		2.474	6.7	7.0	
	7	IL-CJT	1B	2.324	2.310		2.474	6.0	6.6	
			2A	2.312	2.303		2.474	6.6	6.9	
35	1	IL-OWP	1B	2.334	2.323		2.471	5.5	6.0	
			2A	2.334	2.327		2.471	5.6	5.8	
	2	IL-OWP	1B	2.362	2.352		2.471	4.4	4.8	
			2A	2.342	2.338		2.471	5.2	5.4	
	3	IL-BWP	1B	2.337	2.331		2.471	5.4	5.7	
			2A	2.292	2.286		2.471	7.2	7.5	
	4	IL-BWP	1B	2.329	2.324		2.471	5.8	6.0	
			2A	2.293	2.287		2.471	7.2	7.5	
	5	OL-OWP	1B	2.357	2.354		2.471	4.6	4.7	
			2A	2.335	2.330		2.471	5.5	5.7	
	6	OL-BWP	1B	2.341	2.334		2.471	5.3	5.5	
			2A	2.304	2.298		2.471	6.8	7.0	
	7	IL-CLJT	1B	2.344	2.340		2.471	5.1	5.3	
			2A	2.289	2.284		2.471	7.3	7.6	

Table 8. Test results for Cells 77, 78, and 79

Cell	Core	Location	Lift	Bulk specific gravity			Gmm	Air voids,%		
				Method A	Method C	Corelok		Method A	Method C	Corelok
77	1	IL-OWP	1B	2.346	2.339		2.484	5.6	5.8	
			2A	2.394	2.385		2.484	3.6	4.0	
	2	IL-BWP	1B	2.346	2.334		2.484	5.6	6.0	
			2A	2.338	2.333		2.484	5.9	6.1	
	3	OL-OWP	1B	2.296	2.281		2.484	7.5	8.2	
			2A	2.318	2.312		2.484	6.7	6.9	
	4	OLBWP	1B	2.279	2.266		2.484	8.3	8.8	
			2A	2.308	2.302		2.484	7.1	7.3	
78	1	IL-OWP	1B	2.374	2.369		2.484	4.4	4.6	
			2A	2.381	2.376		2.484	4.1	4.3	
	2	IL-OWP	1B	2.361	2.356		2.484	5.0	5.1	
			2A	2.392	2.388		2.484	3.7	3.8	
	3	IL-BWP	1B	2.330	2.323		2.484	6.2	6.5	
			2A	2.355	2.353		2.484	5.2	5.3	
	4	IL-BWP	1B	2.323	2.316		2.484	6.5	6.8	
			2A	2.384	2.380		2.484	4.0	4.2	
	5	OL-OWP	1B	2.305	2.300		2.484	7.2	7.4	
			2A	2.331	2.326		2.484	6.2	6.4	
	6	OL-BWP	1B	2.260	2.258		2.484	9.0	9.1	
			2A	2.287	2.283		2.484	7.9	8.1	
79	4	IL-OWP	1B	2.344	2.336		2.478	5.4	5.7	
			2A	2.320	2.315		2.478	6.4	6.6	
	5	IL-BWP	1B	2.336	2.330		2.478	5.7	6.0	
			2A	2.289	2.283		2.478	7.6	7.9	
	6	OL-OWP	1B	2.337	2.332		2.478	5.7	5.9	
			2A	2.311	2.307		2.478	6.7	6.9	
	7	OL-BWP	1B	2.316	2.309		2.478	6.5	6.8	
			2A	2.313	2.307		2.478	6.7	6.9	
86	11	IL-OWP	1A			1.998	2.527			21.0
	12	IL-OWP	1A			1.998	2.527			21.0
	13	IL-BWP	1A			1.949	2.527			22.9
	14	IL-BWP	1A			1.940	2.527			23.2
	15	OL-OWP	1A			1.990	2.527			21.2
	16	OL-OWP	1A			2.020	2.527			20.0
88	1	IL-OWP	1A			2.077	2.527			17.8
	2	IL-OWP	1A			2.072	2.527			18.0
	3	IL-BWP	1A			2.070	2.527			18.1
	4	IL-BWP	1A			2.068	2.527			18.2
	5	OL-OWP	1A			1.997	2.527			21.0
	6	OL-BWP	1A			2.010	2.527			20.4

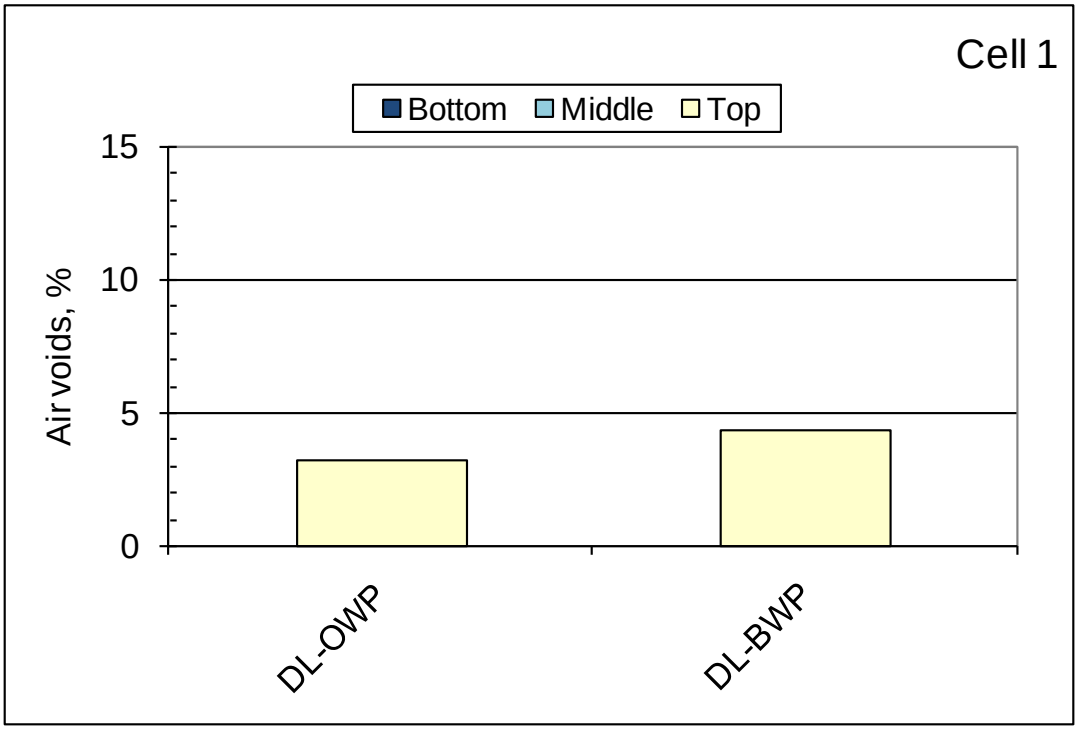

Figure 5. Test results for Cell 1

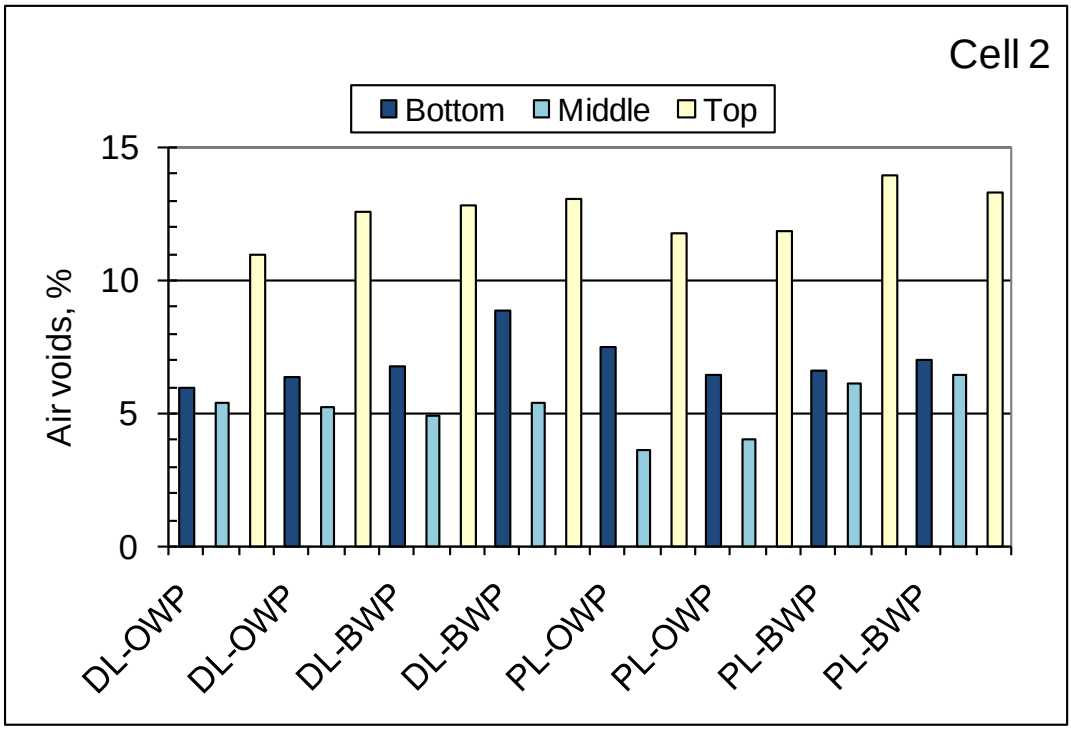

Figure 6. Test results for Cell 2

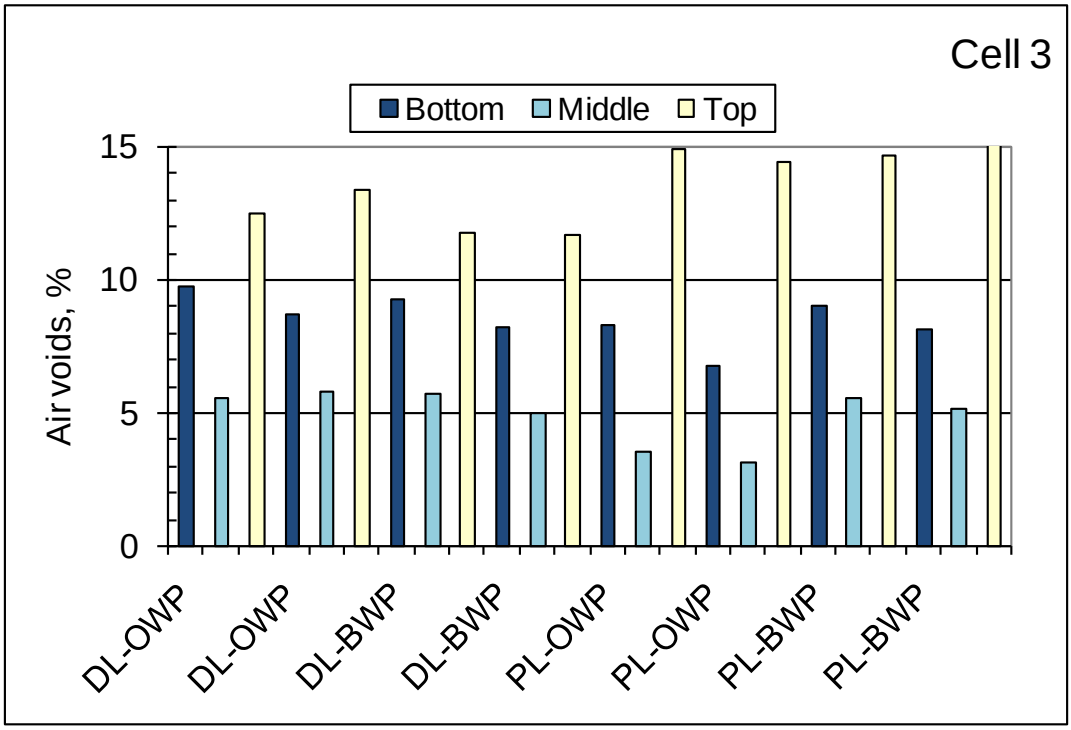

Figure 7. Test results for Cell 3

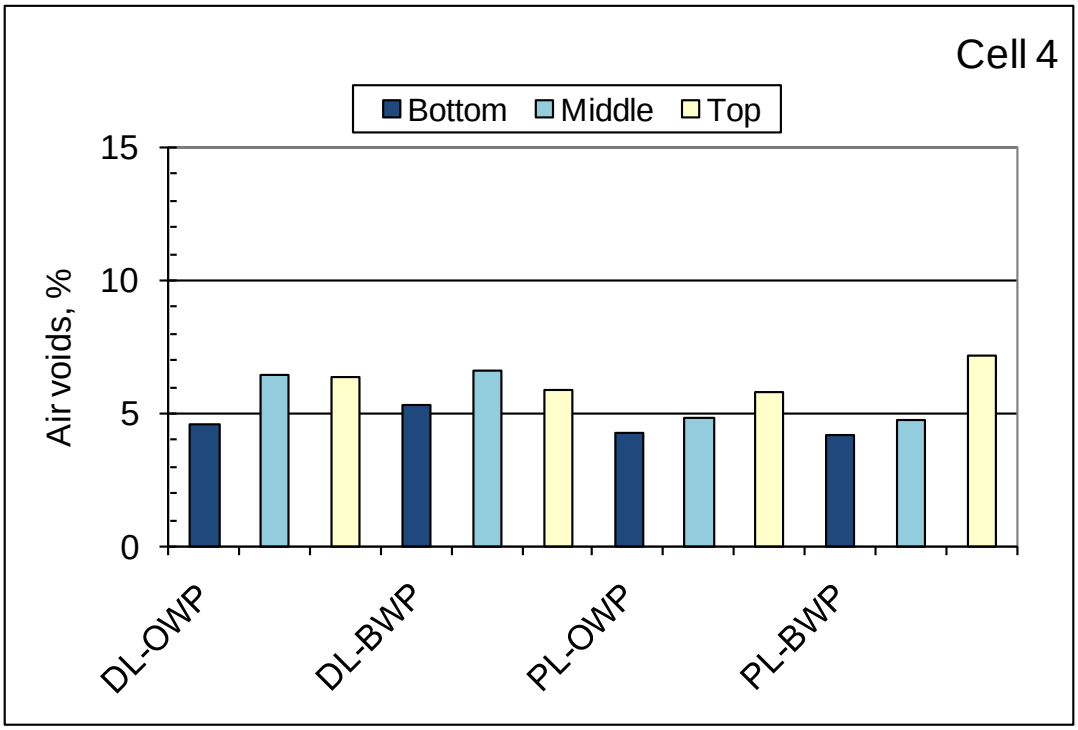

Figure 8. Test results for Cell 4

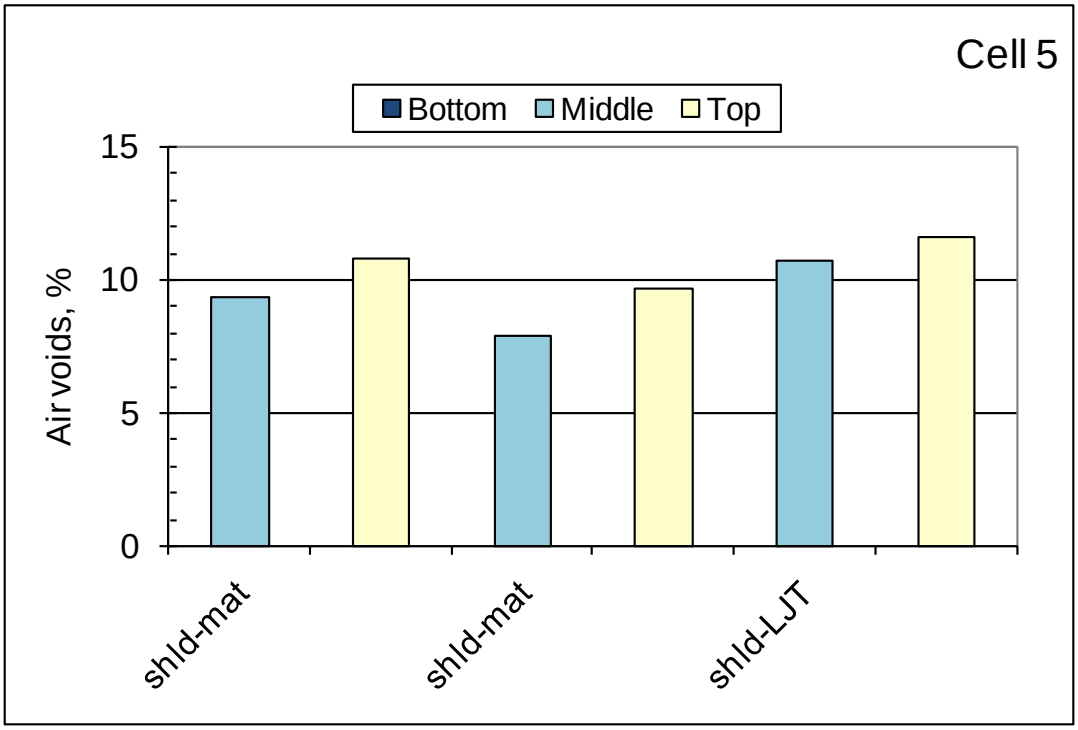

Figure 9. Test results for Cell 5

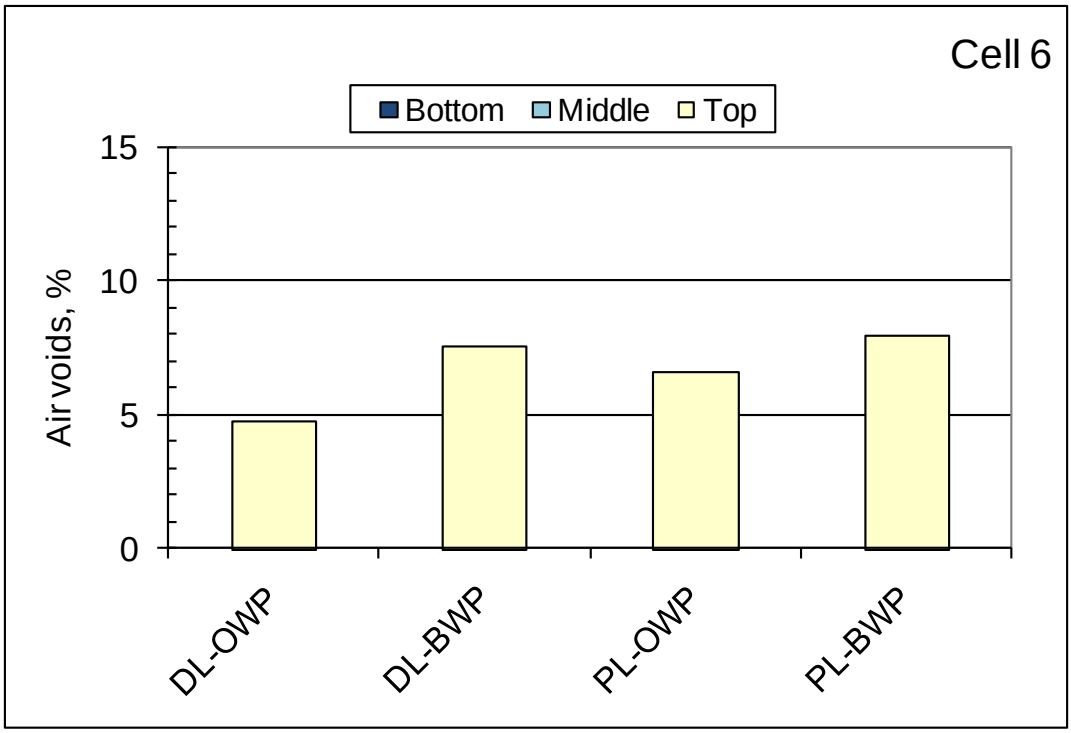

Figure 10. Test results for Cell 6

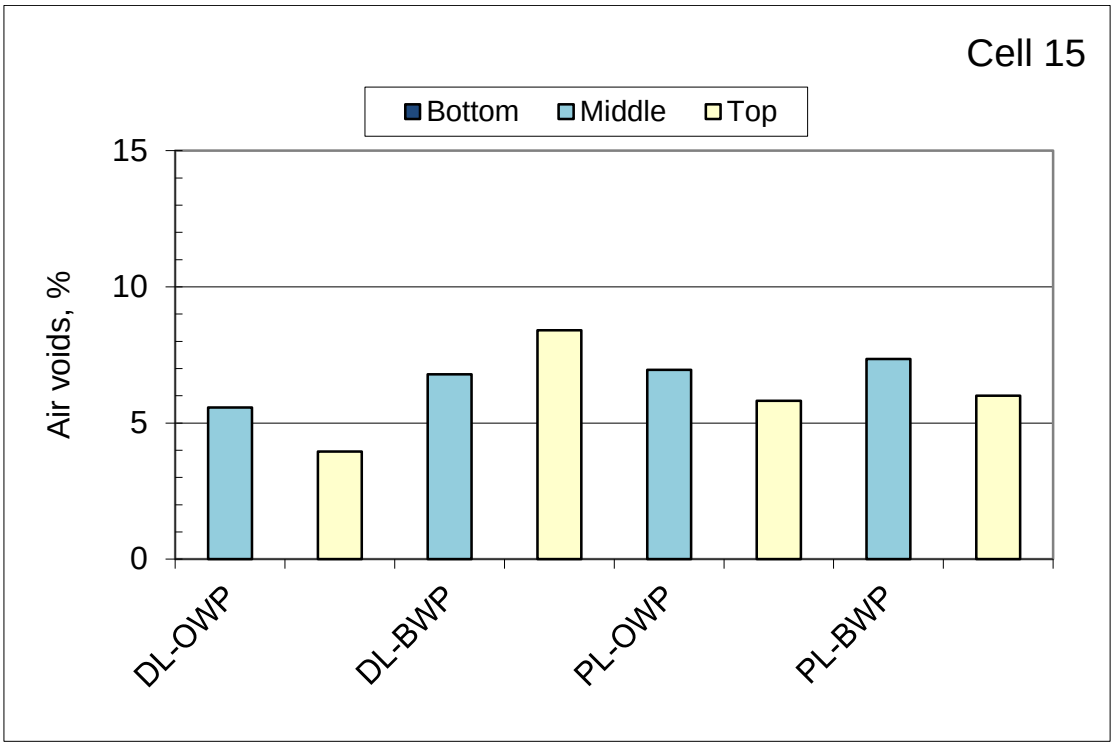

Figure 11. Test results for Cell 15

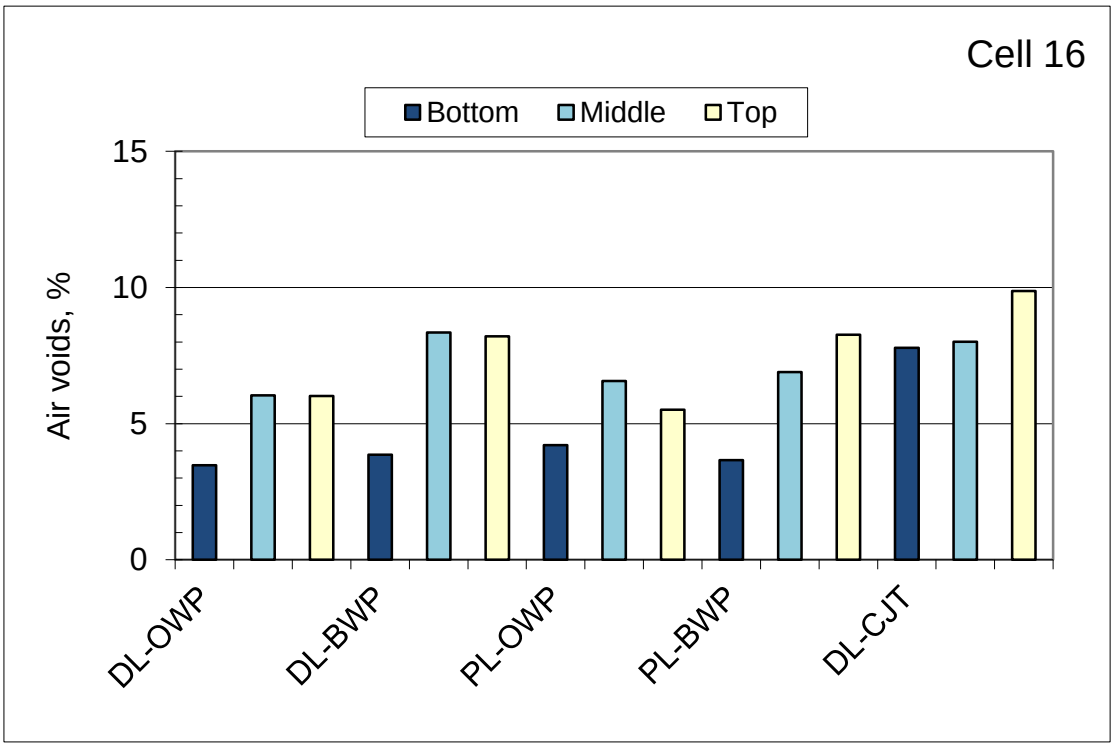

Figure 12. Test results for Cell 16

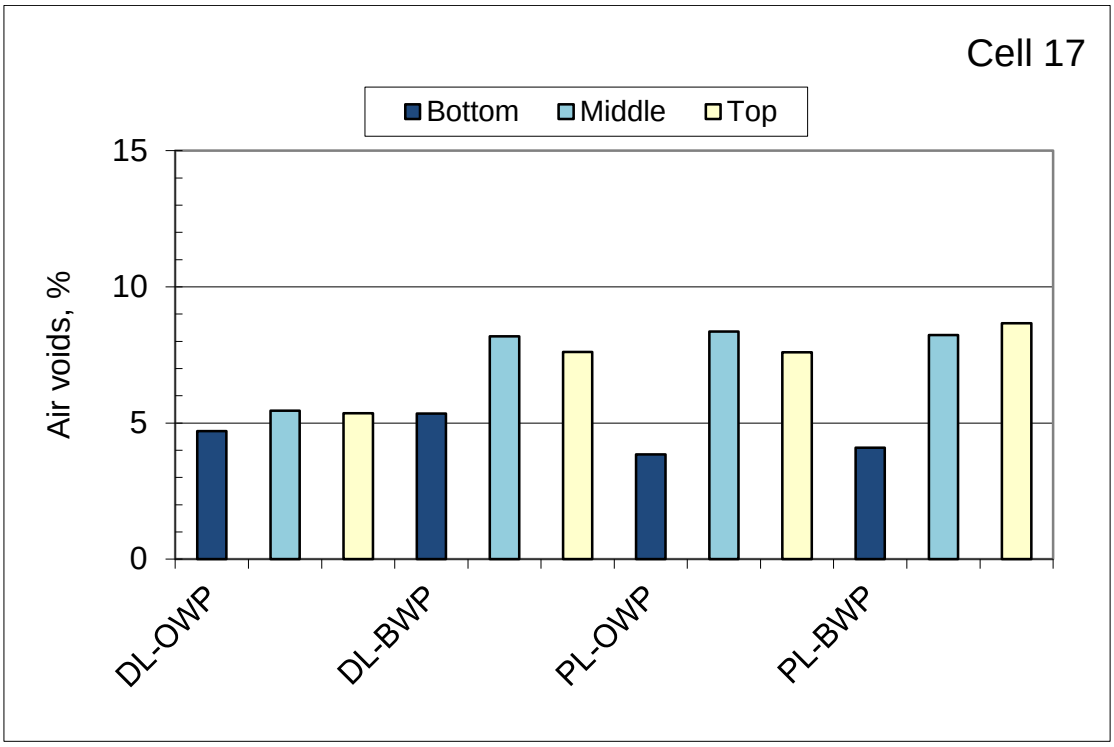

Figure 13. Test results for Cell 17

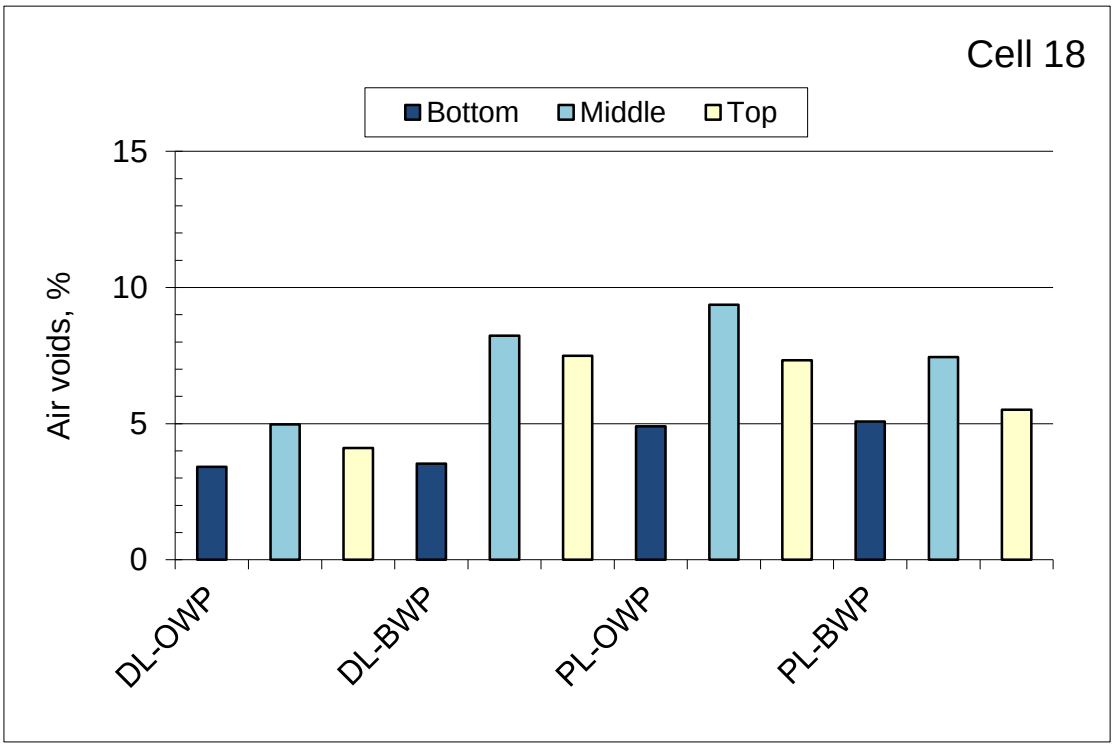

Figure 14. Test results for Cell 18

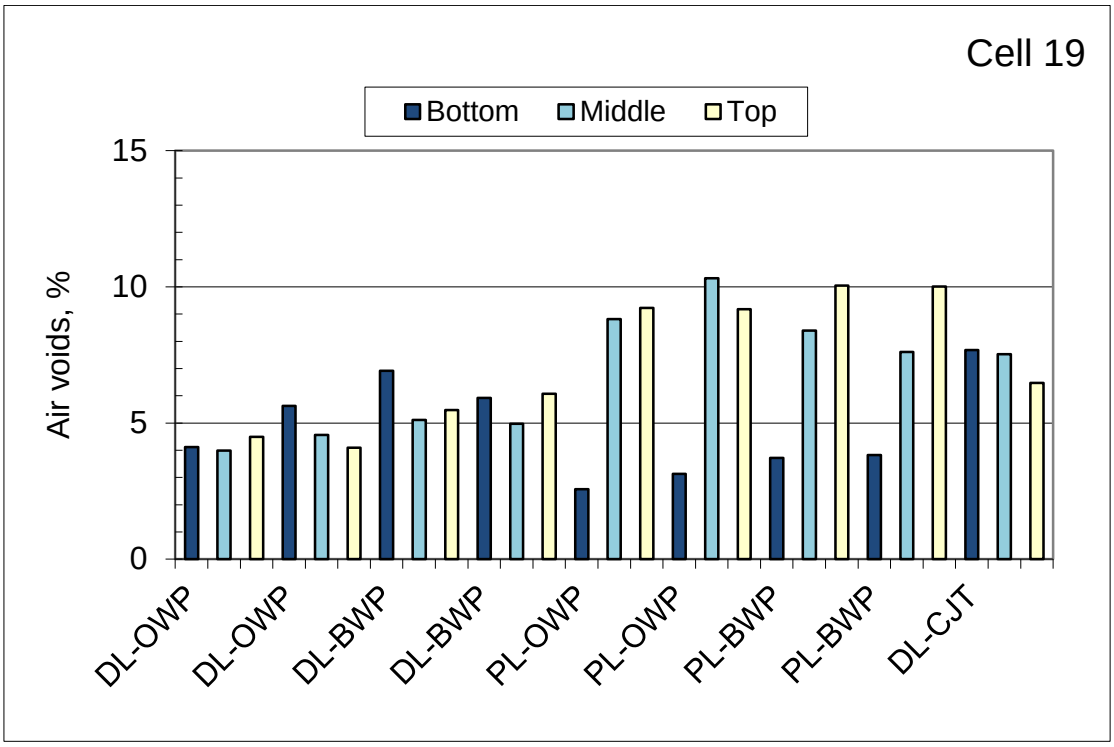

Figure 15. Test results for Cell 19

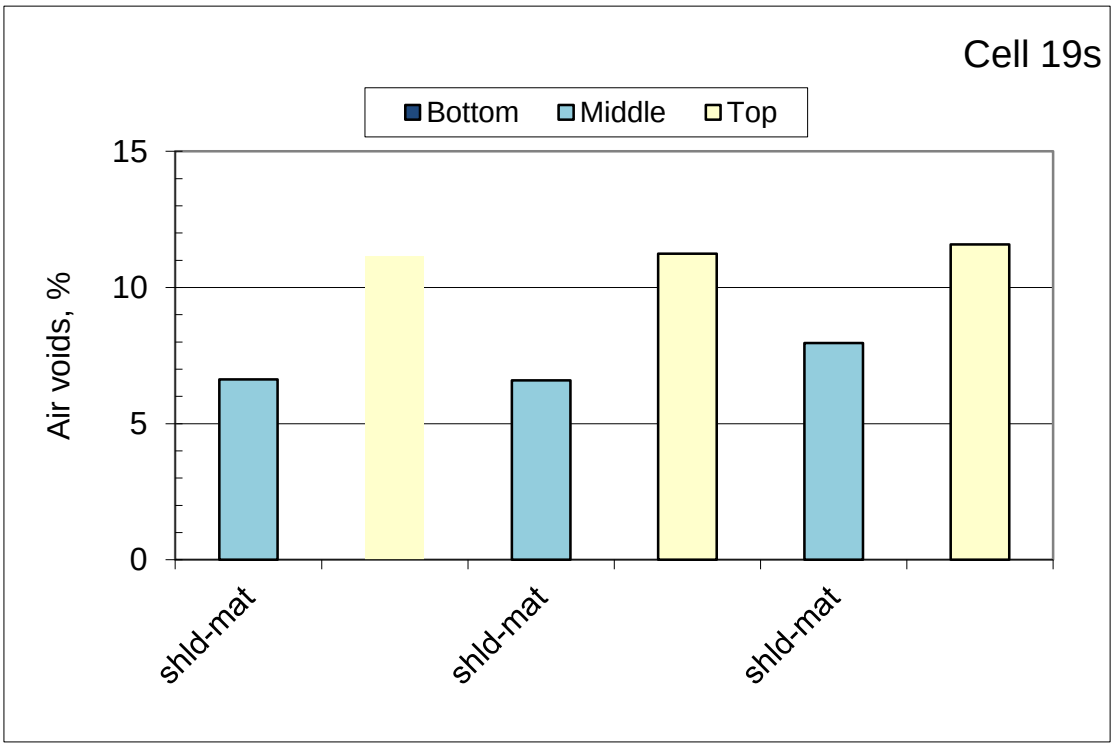

Figure 16. Test results for Cell 19s

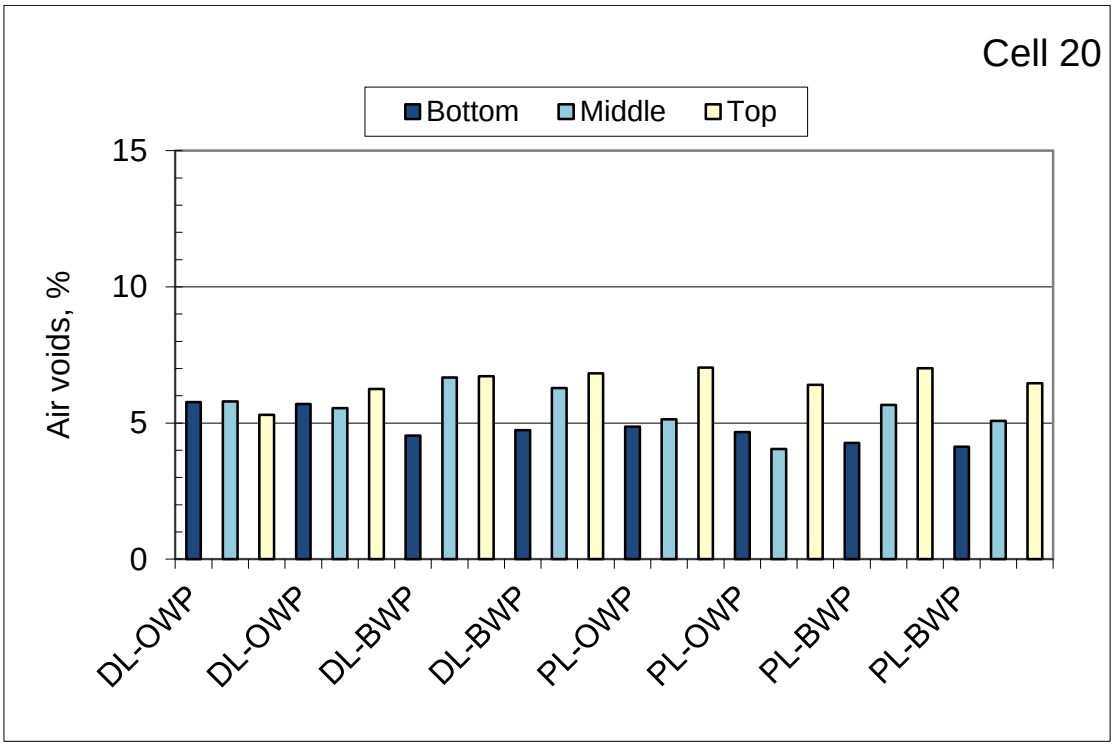

Figure 17. Test results for Cell 20

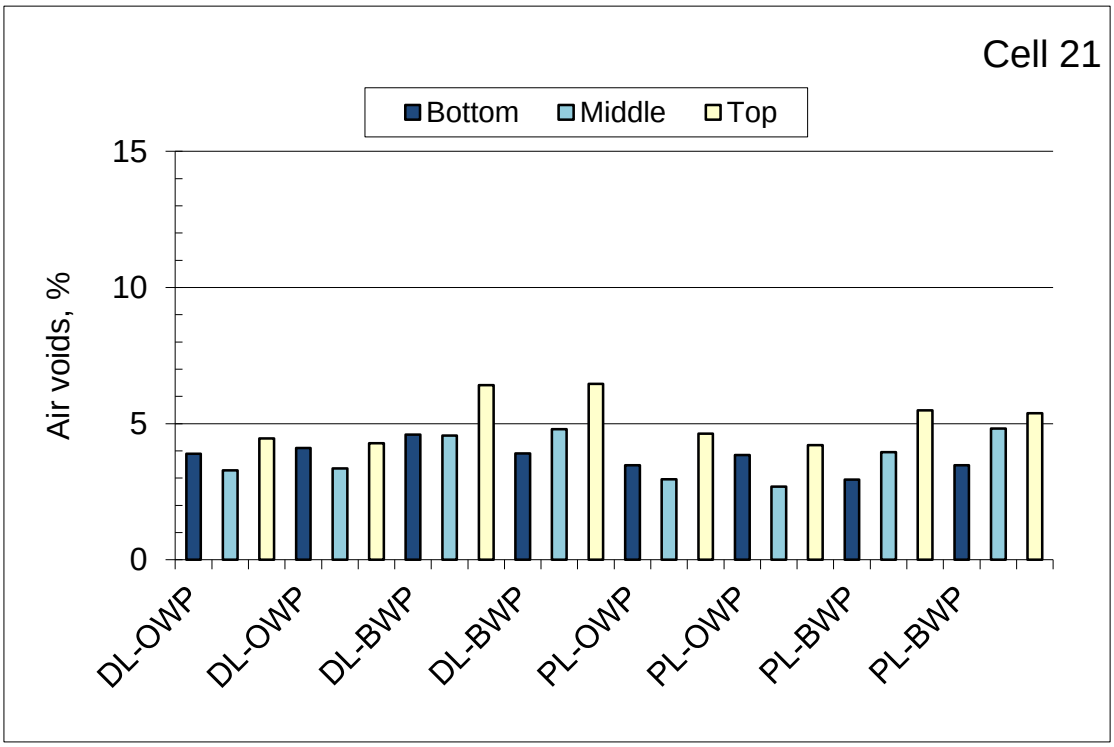

Figure 18. Test results for Cell 21

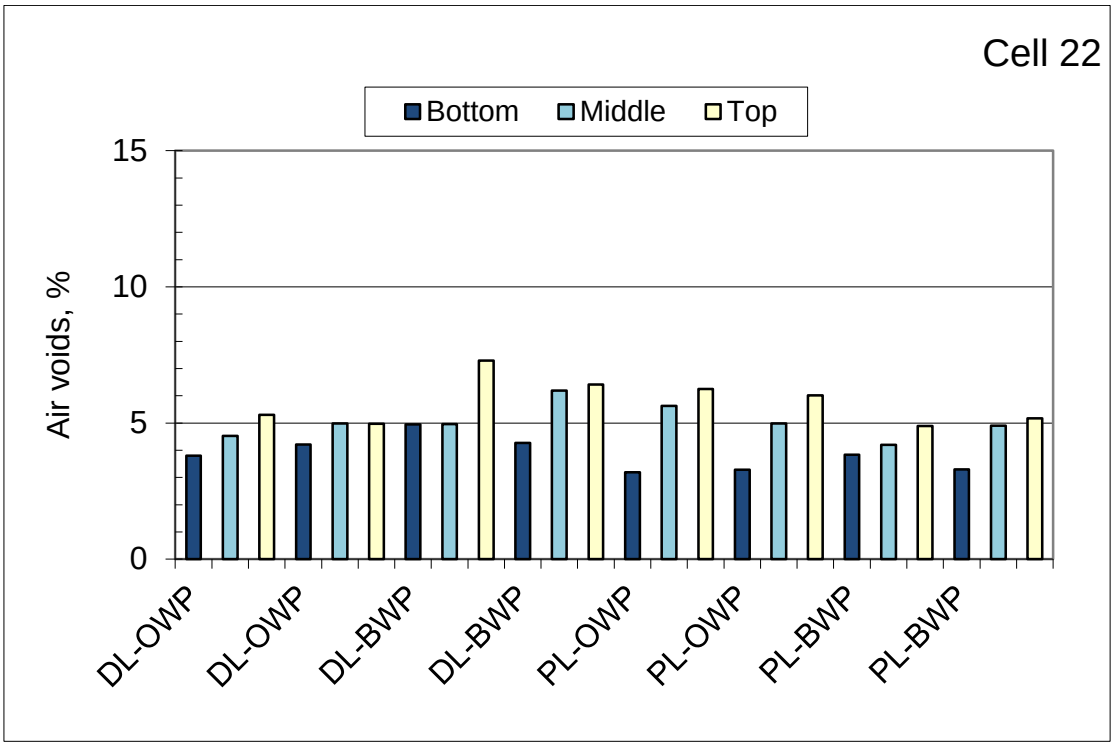

Figure 19. Test results for Cell 22

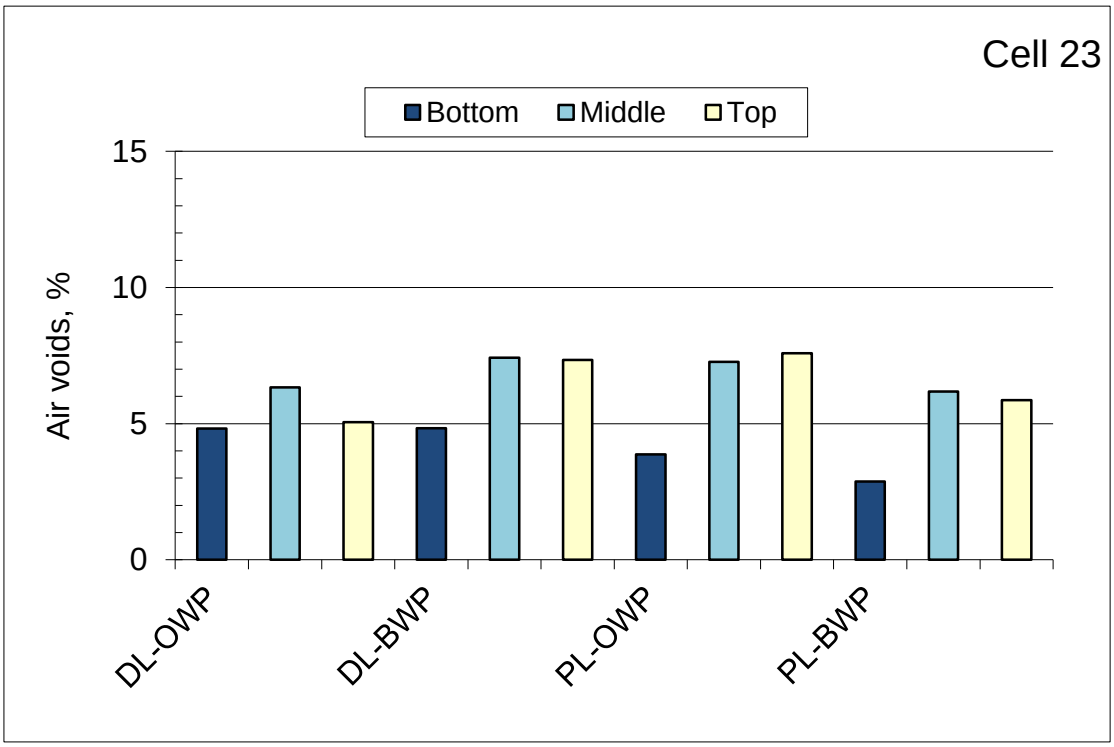

Figure 20. Test results for Cell 23

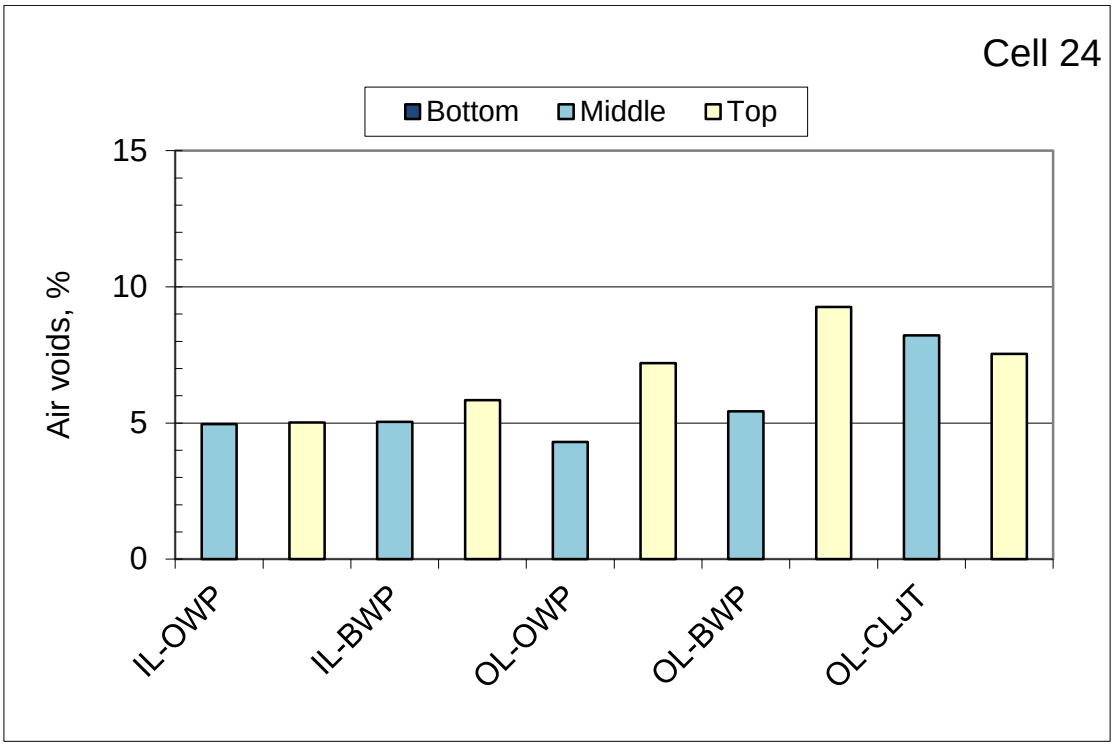

Figure 21. Test results for Cell 24

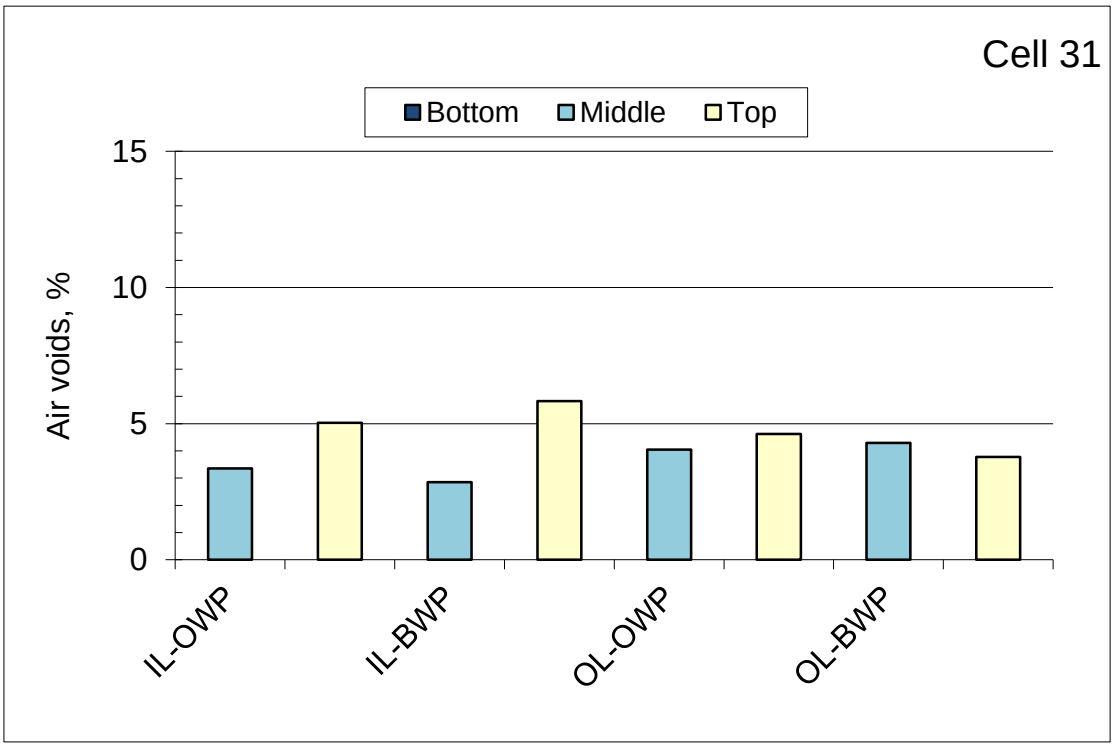

Figure 22. Test results for Cell 31

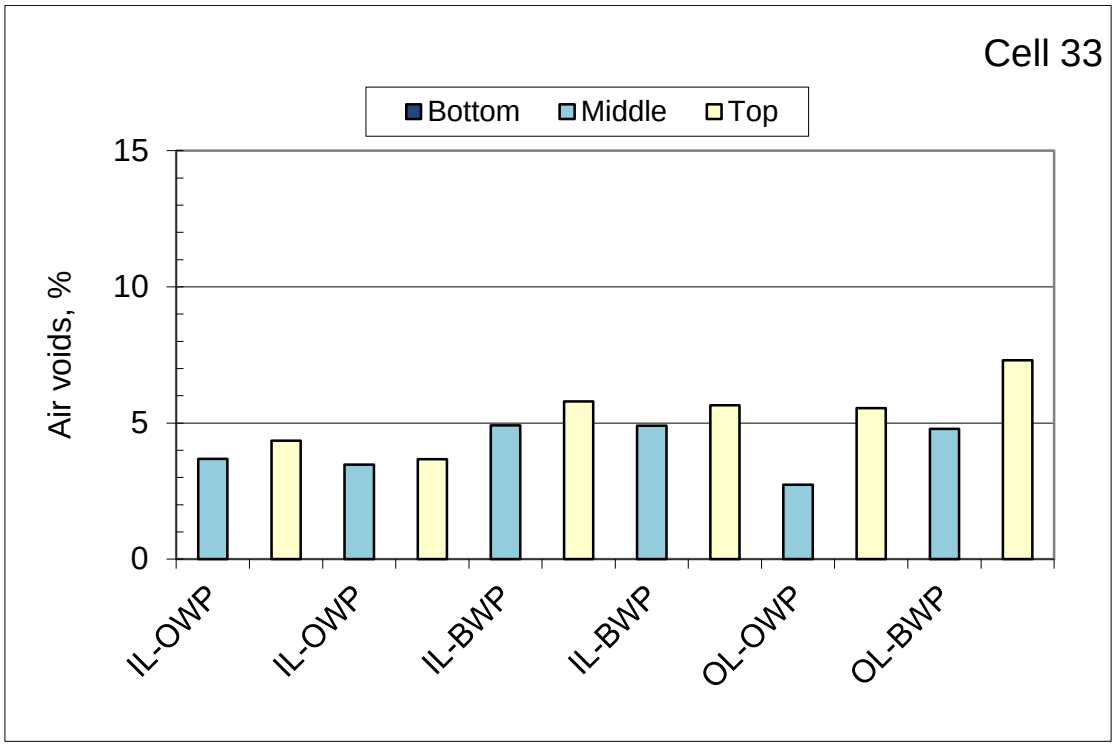

Figure 23. Test results for Cell 33

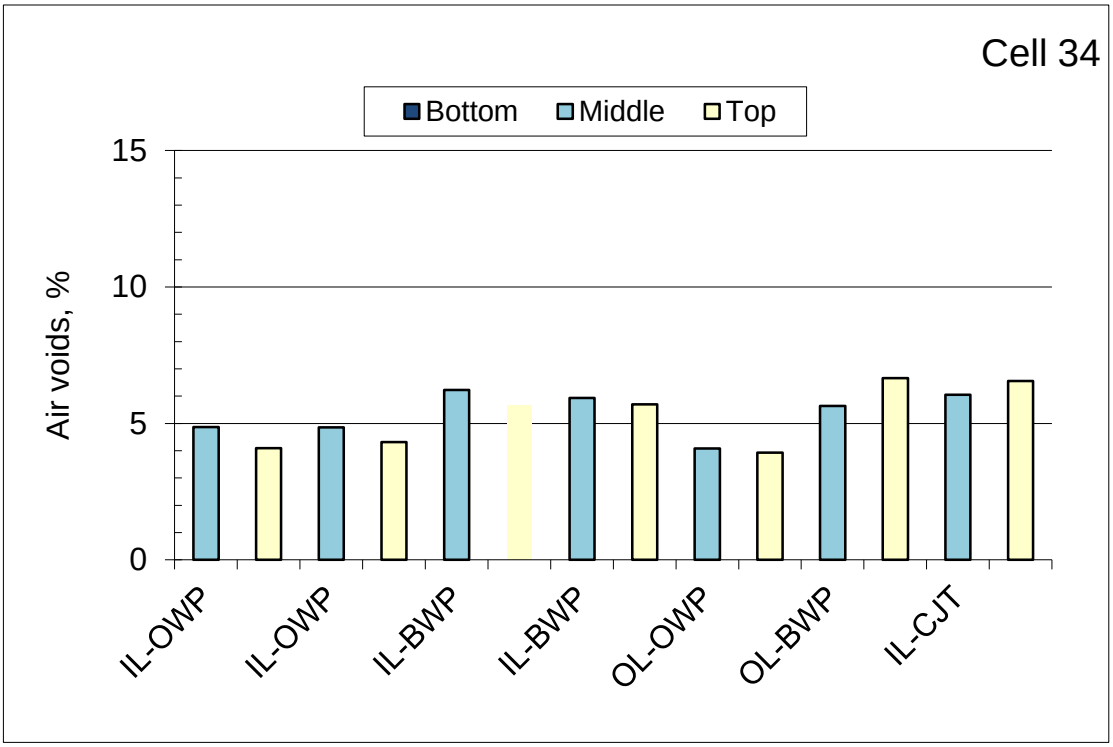

Figure 24. Test results for Cell 34

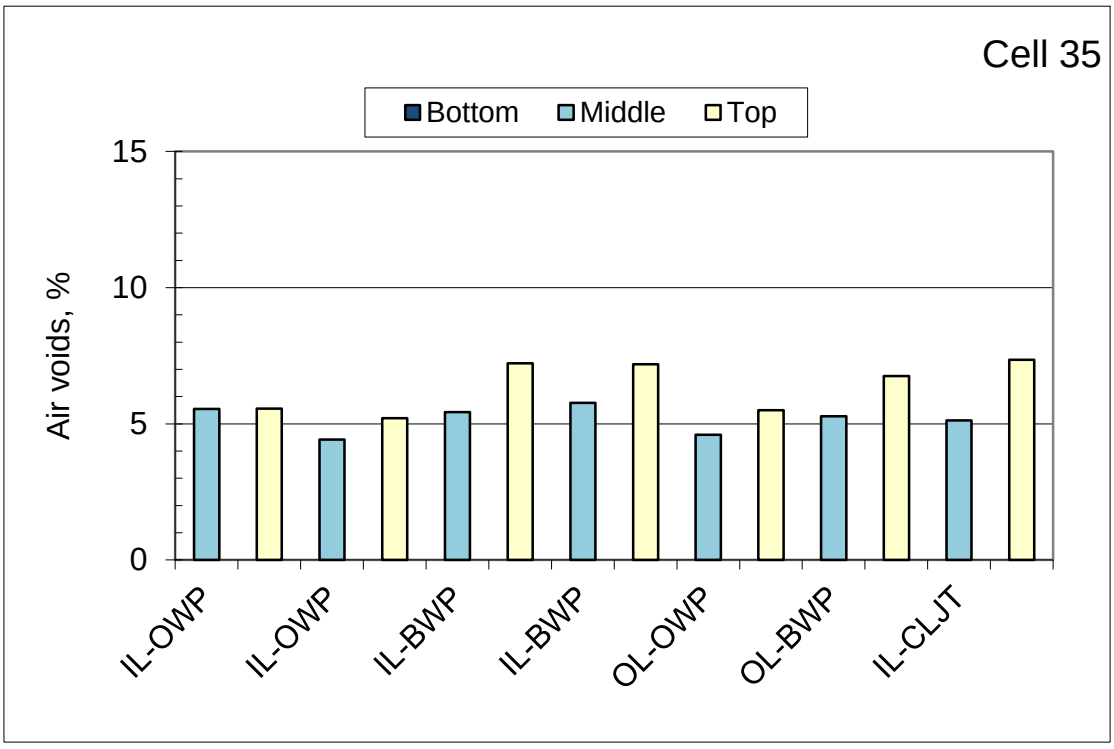

Figure 25. Test results for Cell 35

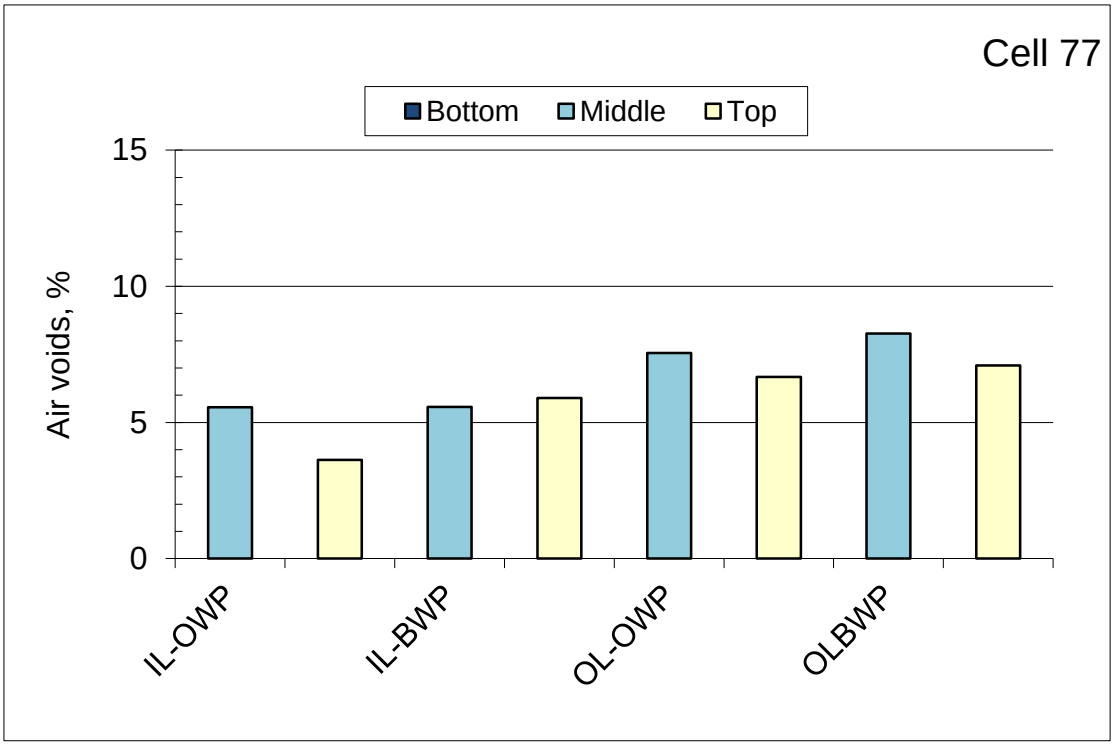

Figure 26. Test results for Cell 77

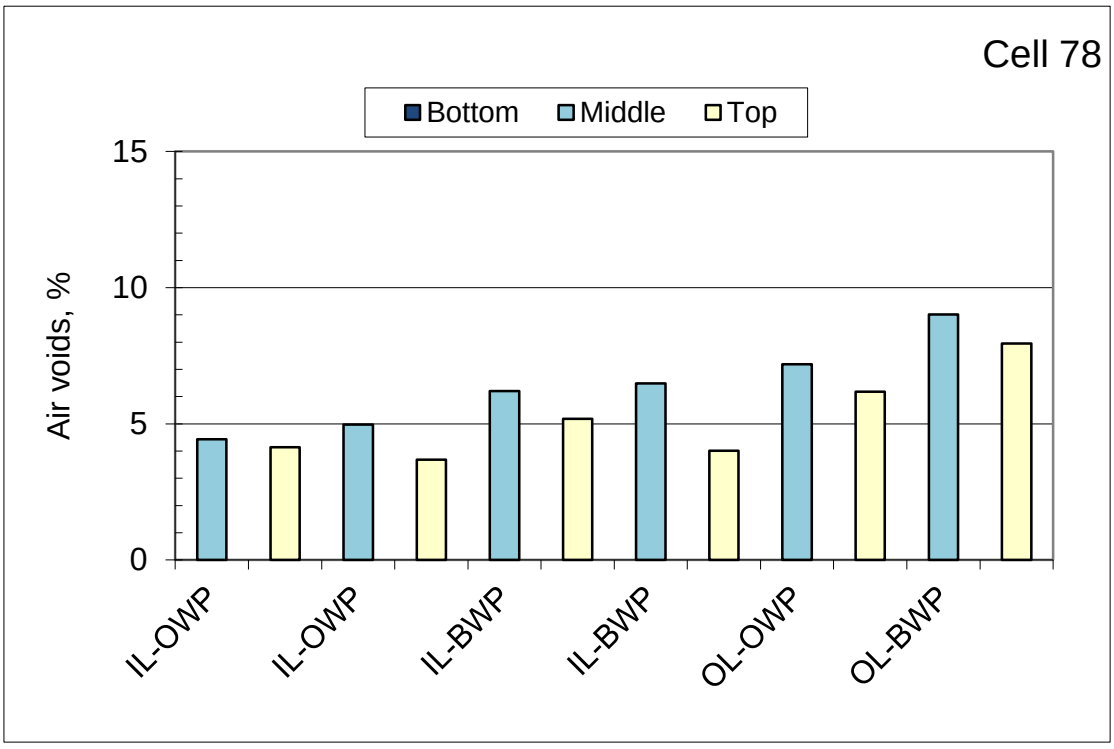

Figure 27. Test results for Cell 78

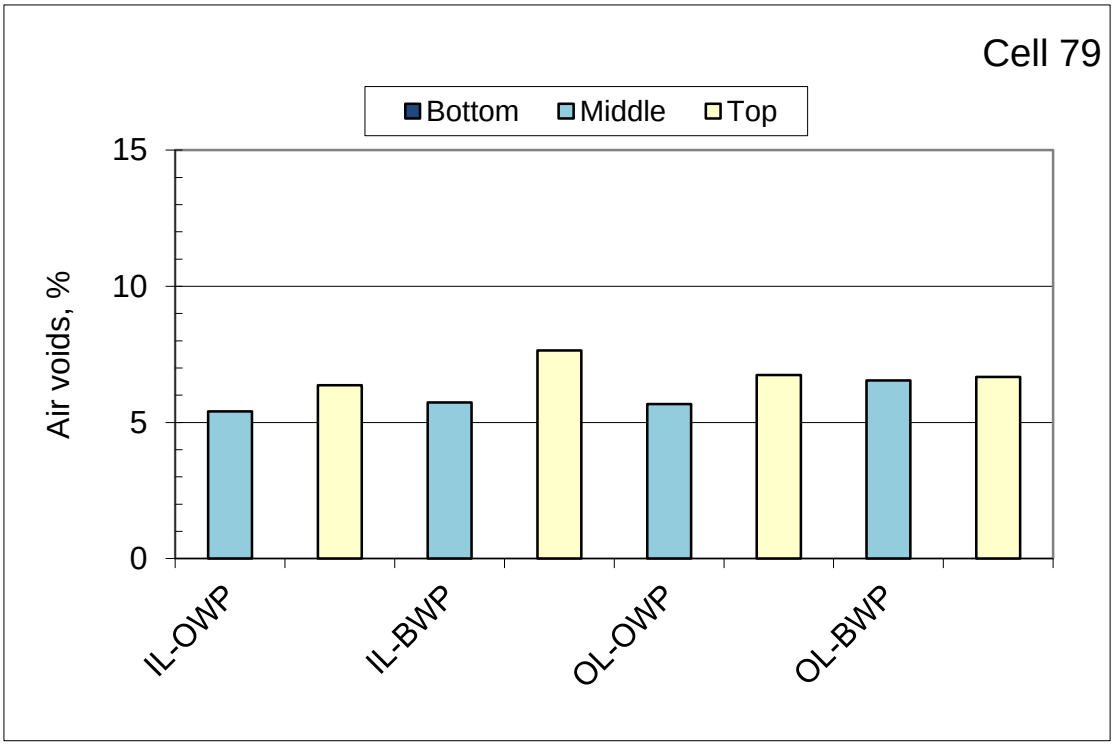

Figure 28. Test results for Cell 79

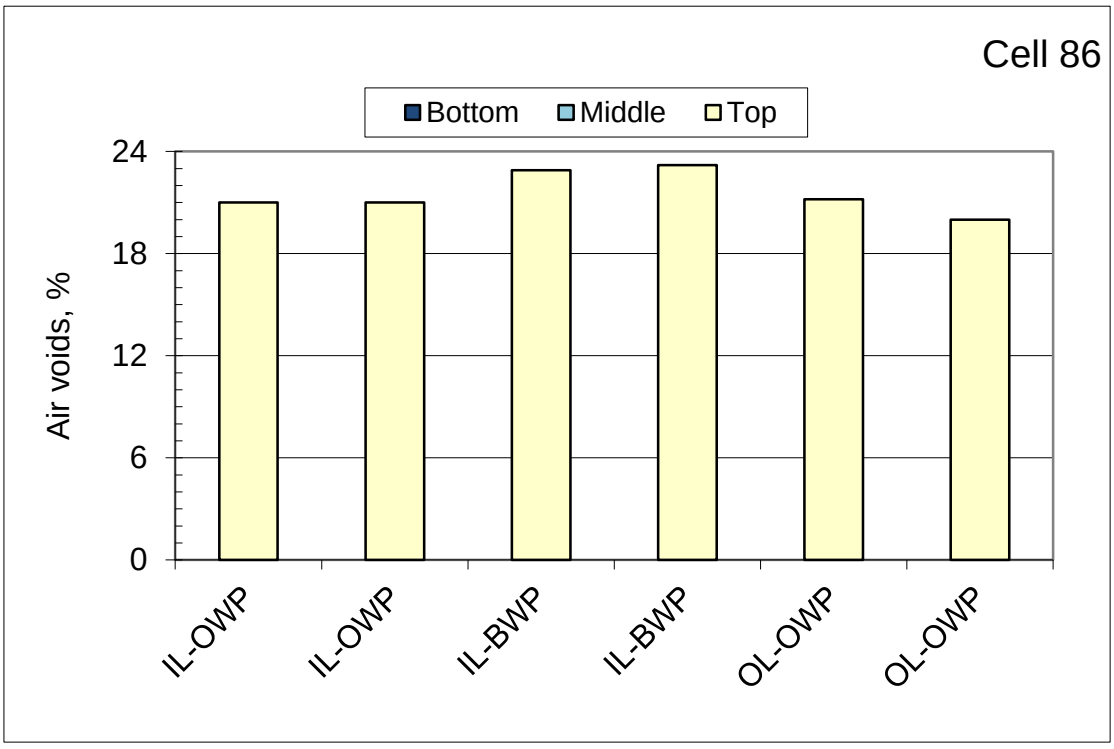

Figure 29. Test results for Cell 86

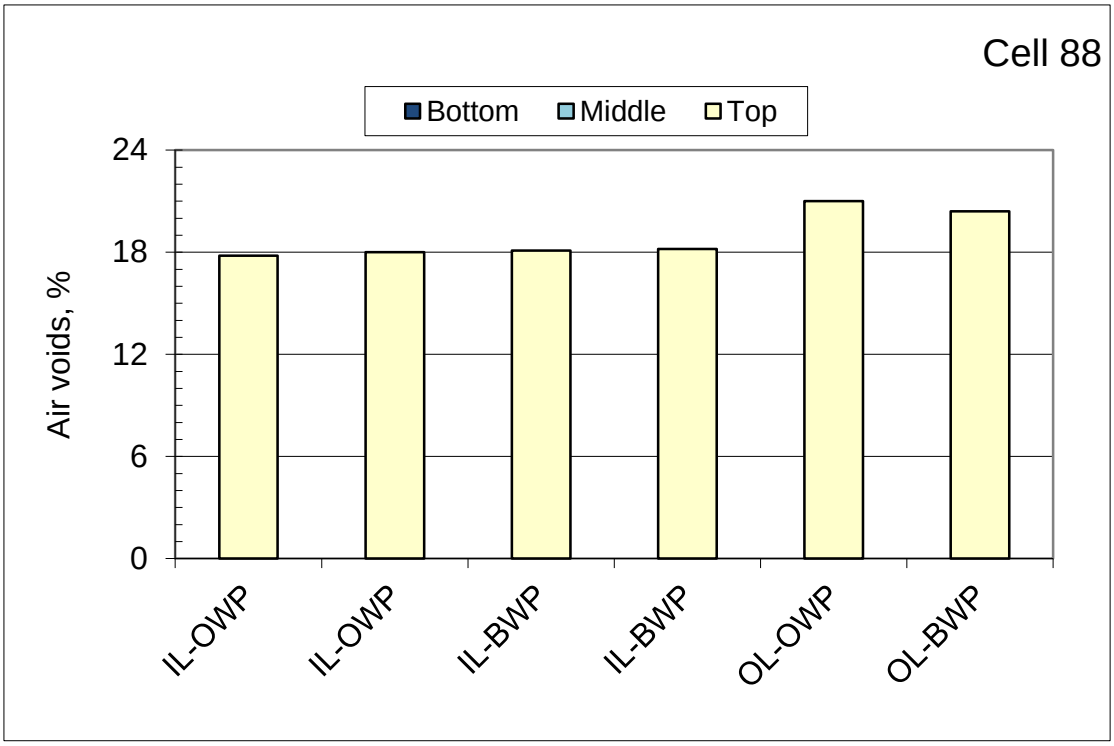

Figure 30. Test results for Cell 88

APPENDIX A: DIGITAL IMAGING ANALYSIS

Additional voids analysis was performed, at no cost to the project, using a method developed at the University of Minnesota (UMN). All samples were scanned on both faces using a regular digital scanner. The files containing the images were copied on two CD's and were delivered to MnDOT. Some of the images obtained were processed with the image processing tool in MATLAB, which stores an image as a matrix of intensity values based on the pixels of the image. When the image is transformed into a binary image, all the pixels have intensity value of either 1 (white) or 0 (black). For asphalt mixtures, aggregates larger than 75 microns are represented by white pixels whereas voids, asphalt binder, and aggregates smaller than 75 microns are represented by black pixels. This distribution can be exploited to calculate the VMA of a mix by using various image processing tools. An example is described below.

Step 1

The back and front surfaces of the core are scanned using a regular scanner and a resolution of 720 dpi**.** Examples are shown in Figures A1 and A2.

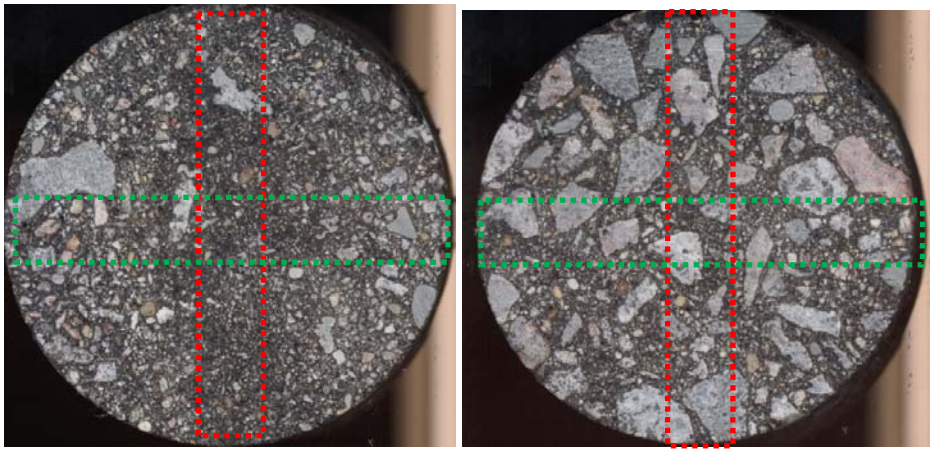

Figure A1. Front and back scanned images, cell 4, core 2, lift 1C

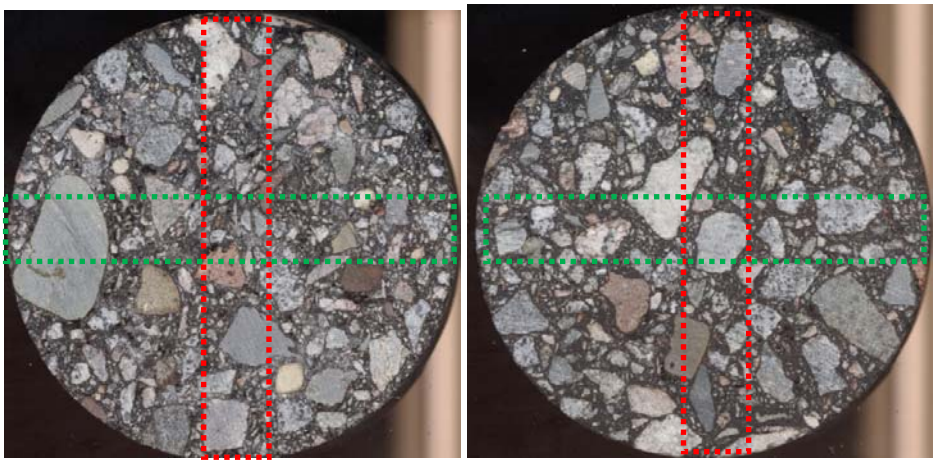

Figure A2. Front and back scanned images, cell 19, core 8, lift 1C

Two cropped images (horizontal and vertical direction) were generated from each scanned image, as shown in Figures A1 and A2, to be able to use a digital imaging method developed in a

different project for scanning BBR mixture beams. If additional funding becomes available, the method can be extended to the entire surface of the core, using either the method developed at University of Minnesota or the method proposed by University of Wisconsin at the asphalt mixture ETG meeting in February 2010.

Step 2

The images are imported in MATLAB and then are converted to gray scale using filtering correction.

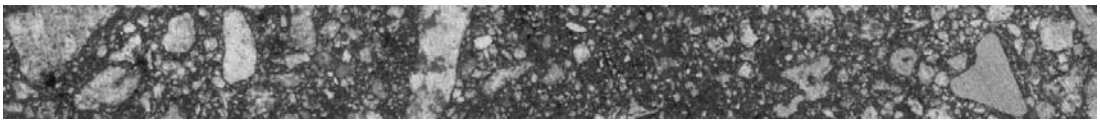

Figure A3. Gray scale image, cell 4, front-horizontal

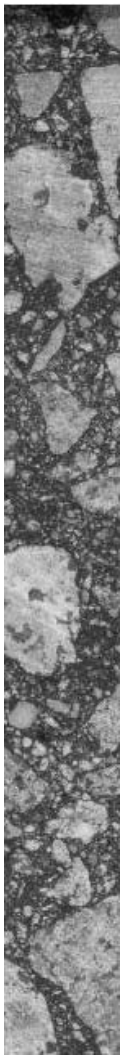

Figure A4. Gray scale image, cell 4, back-vertical

The images are further processed and transformed into binary images, as shown in Figures A5 and A6.

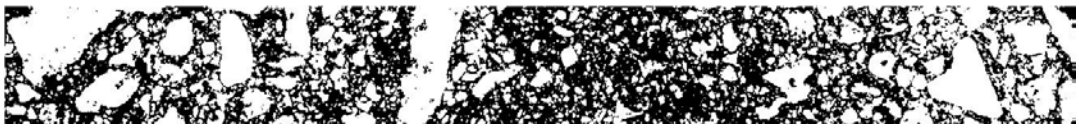

Figure A5. Binary image, cell 4, front-horizontal

Figure A6. Binary image, cell 4, back-vertical

Step 3

VMA is then computed as

$$VMA = \frac{\text{Number of black pixels}}{\text{Total number of pixels}} \times 100 \qquad [1]$$

The results for the four samples are given in Table A1.

Table A1. Calculated VMA values for the four scanned beam specimens

Plate	VMA(%)				
	Front (Horizontal)	Front (Vertical)	Back (Horizontal)	Back (Vertical)	**Average**
Cell 4, core 2, lift 1C	46.2	62.1	32.8	34.4	**43.9**
Cell 19, core 8, lift 1C	30.3	29.5	33.7	35.8	**32.3**

One drawback of this method is that aggregates smaller than 75 microns, along with binder and air voids, are represented as black pixels (intensity value of 0). The aggregates greater than 75 microns are represented as white pixels (intensity value of 1). Therefore, aggregates smaller than 75 microns act as an additional component in the computation of VMA and result in higher VMA values.

At the given resolution it is not possible to separate the aggregates less than 75 microns from the binder and void pixels. However, if the aggregate gradation of the mix is known or can be calculated, it is possible to calculate the ratio of aggregates larger than 75 microns to aggregates smaller than 75 microns. This ratio is termed the "volume ratio" and is defined as follows:

$$\text{Volume Ratio} = \frac{\text{Vol. of aggregates} > 75\ \text{microns}}{\text{Vol. of aggregates} < 75\ \text{microns}} \qquad [2]$$

For a digital scanned image, the volume of a phase is representative of its surface area. Since the total number of aggregates larger than 75 microns can be calculated from the digital binary image, the number of pixels associated with aggregates smaller than 75 microns can also be estimated based on the volume ratio. Therefore, a corrected VMA is obtained as:

$$\text{VMA}_C = \frac{\text{No. of black pixels} - \text{No. of pixels of aggregates} \le 75\ \text{microns}}{\text{Total no. of pixel in the image}} \times 100 \qquad [3]$$

Consider for example cell 4, core 2, lift 1C front-horizontal case. Applying equation [1] the following result is obtained:

$$VMA = \frac{228469}{752400} \times 100 = 30.3\%$$

Let's assume two volume ratio values, 3 and 7, respectively. For volume ratio 3, the following calculations can be performed:

$$VolumeRatio = 3 = \frac{228469}{x}, \therefore x = 76156$$

and the following corrected VMA value is obtained:

$$VMA_C = \frac{228469 - 76156}{752400} \times 100 = 20.2\%$$

For volume ratio 7, the following calculations can be performed

$$VolumeRatio = 7 = \frac{228469}{x}, \therefore x = 32638$$

and the following corrected VMA value is obtained:

$$VMA_C = \frac{228469 - 32638}{752400} \times 100 = 26.0\%$$

Table A2 summarizes the results.

Table A2. VMA values corrected for presence of fines

VMA uncorrected (%)	VMA corrected (%)	
	Volume Ratio = 3	Volume Ratio = 7
30.3	20.2	26.0

APPENDIX B: ULTRASONIC TESTING

Ultrasonic testing of field sections was performed as part of a separate FHWA study by Kyle Hoegh and Dr. Lev Khazanovich. Preliminary research at University of Minnesota suggests that an increased air void content causes lower shear wave velocity. Further testing and calibration must be conducted in order to verify this technology as viable for implementation. It should also be noted that the ultrasonic testing can only be applied in the field or on specimens with a large surface area to eliminate boundary effects on the signal interpretation, and testing should only be conducted when the asphalt is not exposed to sun-drenching.

This document summarizes the results testing with an ultrasound tomography device (MIRA) for an asphalt (cell 33) and concrete (cell 52) pavement section. Testing was conducted March 17th and 18th on the low volume loop of the Minnesota road research facility (MnROAD) near Minneapolis, MN. Ultrasonic measurements were taken to supplement ground penetrating radar (GPR) measurements.

Measurement Procedure

GPR measurements had previously been taken with the outside of the antenna right at the inside edge of the paint stripe and the center of the CMP banks at 1 ft, 3 ft, and 5 ft from the inside edge of this "fog line" white paint strip of Cells 33 and 52. Three sets of 20 ft locations were made at both Cells 33 and 52 with MIRA as follows to supplement the information gathered by the GPR:

1. "Beginning 1": 1 ft from the inside edge of the paint strip, starting at 2 ft from the beginning of the section, 10 measurements, 2 ft apart.
2. "Beginning 5": 5 ft from the inside edge of the paint strip, starting at 2 ft from the beginning of the section, 10 measurements, 2 ft apart.
3. "End 1": 1 ft from the inside edge of the paint strip, starting at 2 ft from the end of the section, 10 measurements, 2 ft apart.

The scans were centered at each location with the long portion of the device aperture perpendicular to the direction of traffic and the right side of the device and corresponding right side of the scan output closest to the paint strip for beginning locations and the left side of the scan output closest to the paint strip for the end locations. Five scans were taken at all locations with the 3rd scan directly over the marking. A video showing an example of the 5 scan process at each location can be viewed by holding down "Ctrl" and clicking on link 1 (note: all links require internet access). Additional scanning locations in close proximity had to be added at one location (ID: Cell 52-13) to avoid a surface crack at the measurement location (see link 2).

Data Interpretation

The relevant information for each measurement location in cells 33 and 52 is shown in tables B1 and B2, respectively. The excel documents containing this information can also be downloaded at link 3 and link 4, respectively. The shear wave velocity and corresponding pavement thickness was determined at each measurement location, excluding measurement location "Cell 52 – 1" (more on this location in the "future work" section of this report).

Table B1. Cell 33 measurement location IDs and corresponding information link 3

Measurement Identification	Measurement location	From the beginning of the section, ft	from inside edge of the paint stripe, ft	location w/ respect to the cell	pavement thickness, mm	Velocity, m/s	Comments
Cell 33-1	1	2	1	beginning	108	2131	asphalt drenched from earlier rain current light drizzle temperature at mid 30s fahrenheit
Cell 33-2	2	4	1	beginning	103	2142	
Cell 33-3	3	6	1	beginning	104	2136	
Cell 33-4	4	8	1	beginning	105	2136	
Cell 33-5	5	10	1	beginning	103	2129	
Cell 33-6	6	12	1	beginning	97	2136	
Cell 33-7	7	14	1	beginning	94	2151	
Cell 33-8	8	16	1	beginning	92	2158	
Cell 33-9	9	18	1	beginning	88	2146	
Cell 33-10	10	20	1	beginning	92	2154	
Cell 33-11	1	2	5	beginning	107	2095	
Cell 33-12	2	4	5	beginning	101	2082	
Cell 33-13	3	6	5	beginning	98	2096	
Cell 33-14	4	8	5	beginning	101	2085	
Cell 33-15	5	10	5	beginning	99	2089	
Cell 33-16	6	12	5	beginning	99	2089	
Cell 33-17	7	14	5	beginning	97	2090	
Cell 33-18	8	16	5	beginning	102	2081	
Cell 33-19	9	18	5	beginning	101	2078	
Cell 33-20	10	20	5	beginning	94	2085	
Cell 33-21	1	2	1	end	82	1996	measurements taken in afternoon after surface is mostly dried temperature in mid 40s fahrenheit
Cell 33-22	2	4	1	end	80	1995	
Cell 33-23	3	6	1	end	84	2013	possible deterioration at thickness interface
Cell 33-24	4	8	1	end	85	1998	
Cell 33-25	5	10	1	end	79	2008	
Cell 33-26	6	12	1	end	82	1989	
Cell 33-27	7	14	1	end	85	1975	
Cell 33-28	8	16	1	end	89	1988	
Cell 33-29	9	18	1	end	85	1988	
Cell 33-30	10	20	1	end	83	2007	

Table B2. Cell 52 measurement location IDs and corresponding information link 4

Measurement Identification	Measurement location	From the beginning of the section, ft	from inside edge of the paint stripe, ft	location w/ respect to the cell	pavement thickness, mm	Velocity, m/s	Comments
Cell 52-1	1	2	1	beginning	-	2696	Bar or void causing a center circular reflection at about 85 mm depth. Additional cracking or embedded object shadowing all backwall reflection
Cell 52-2	2	4	1	beginning	171	2712	Same circular reflection on left (-40 mm). Shadowing of back wall reflection less prevalent and moves left in the aperture as you move east)
Cell 52-3	3	6	1	beginning	171	2722	
Cell 52-4	4	8	1	beginning	186	2715	
Cell 52-5	5	10	1	beginning	187	2698	
Cell 52-6	6	12	1	beginning	188	2786	
Cell 52-7	7	14	1	beginning	182	2797	
Cell 52-8	8	16	1	beginning	184	2783	
Cell 52-9	9	18	1	beginning	183	2772	
Cell 52-10	10	20	1	beginning	184	2800	
Cell 52-11	1	2	1	end	159	2750	
Cell 52-12	2	4	1	end	164	2742	
Cell 52-13	3	6	1	end	163	2750	measurements on surface crack replaced with adjacent measurements
Cell 52-14	4	8	1	end	168	2798	
Cell 52-15	5	10	1	end	165	2784	
Cell 52-16	6	12	1	end	168	2763	
Cell 52-17	7	14	1	end	166	2780	
Cell 52-18	8	16	1	end	168	2765	
Cell 52-19	9	18	1	end	166	2753	
Cell 52-20	10	20	1	end	170	2762	
Cell 52-21	1	2	5	beginning	158	2728	something embedded or cracking occuring on the left side. Significant shadwoing as move east
Cell 52-22	2	4	5	beginning	176	2722	similar to meas loc 1 but only minor and at way left
Cell 52-23	3	6	5	beginning	170	2687	
Cell 52-24	4	8	5	beginning	177	2686	
Cell 52-25	5	10	5	beginning	190	2666	
Cell 52-26	6	12	5	beginning	186	2629	
Cell 52-27	7	14	5	beginning	193	2696	
Cell 52-28	8	16	5	beginning	200	2727	
Cell 52-29	9	18	5	beginning	190	2724	
Cell 52-30	10	20	5	beginning	190	2744	

In each ultrasonic tomography scan, the pavement thickness was determined by the backwall reflection. Figures B1 and B2 show typical asphalt and concrete scans, respectively (a scan at each measurement location for both cell 33 and 52 can be seen at link 5 and link 6, respectively). The midpoint of the backwall reflection shown in the scans corresponds to the thickness of the pavement layer. The first three readable scans at each location were averaged to assign the pavement thickness at each location. It should be noted that the backwall reflection becomes less and less prominent on the outside portions of each scan due to the effect of limited aperture (less transmitting and receiving pair wavefront paths on the outer edges).

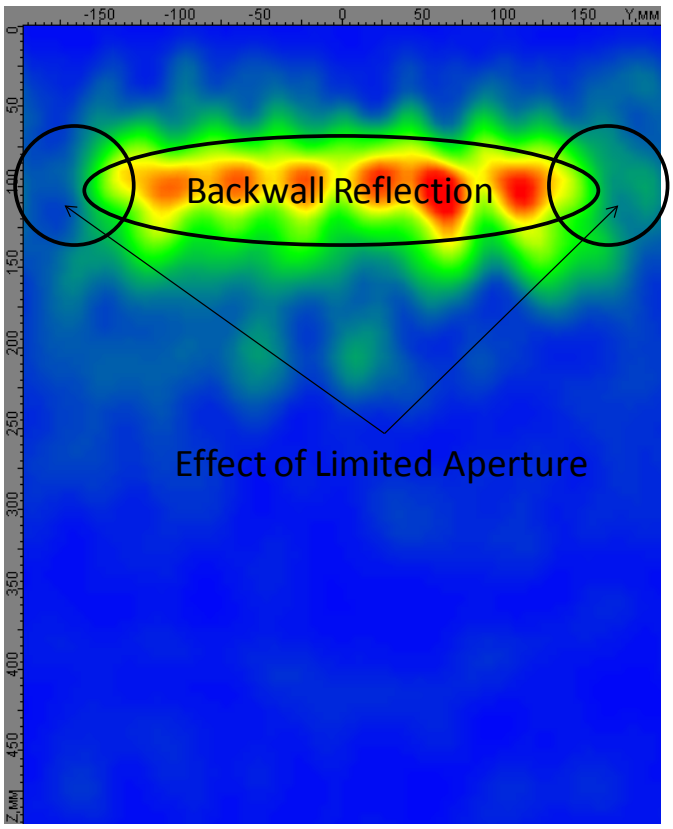

Figure B1. Cell 33 example asphalt pavement thickness backwall reflection link 5

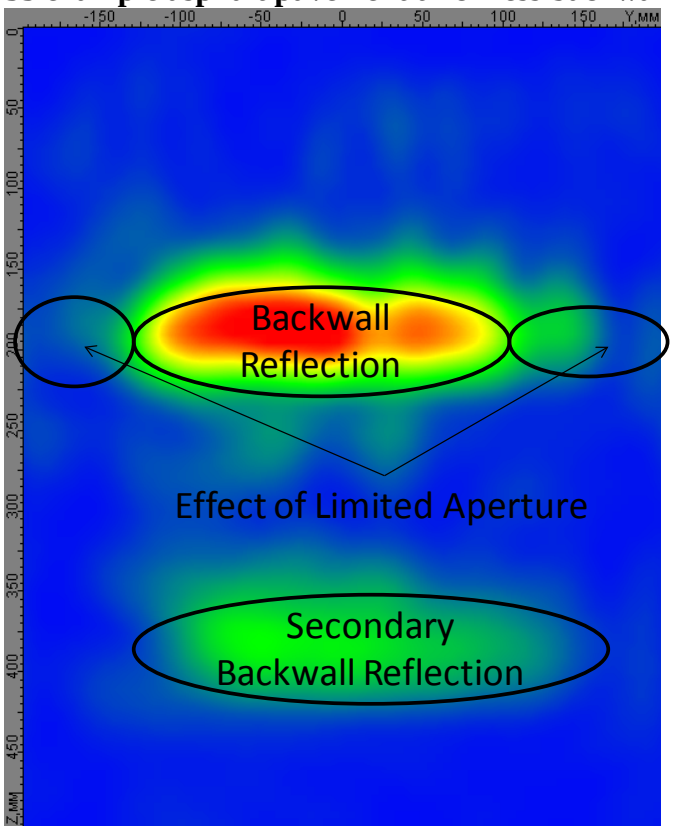

Figure B2. Cell 52 example pcc pavement thickness backwall reflection link 6

Results

Figures B3 and B4 show MIRA measured pavement thickness for the 30 measurement locations in cells 33 and 52, respectively. The measurements are displayed in the three groups described in the introduction (Beginning 1, Beginning 5, and End 1). The measurements were taken at 2 ft. intervals centered 1 or 5 ft. from the longitudinal joint in Cell 33 and Cell 52. The MIRA measured thicknesses ranged from 78 mm to 108 mm in Cell 33 and 158 mm to 200 mm in Cell 52. It can be observed that the end of the section was significantly shallower in pavement thickness than the beginning of the section for both pavement cells.

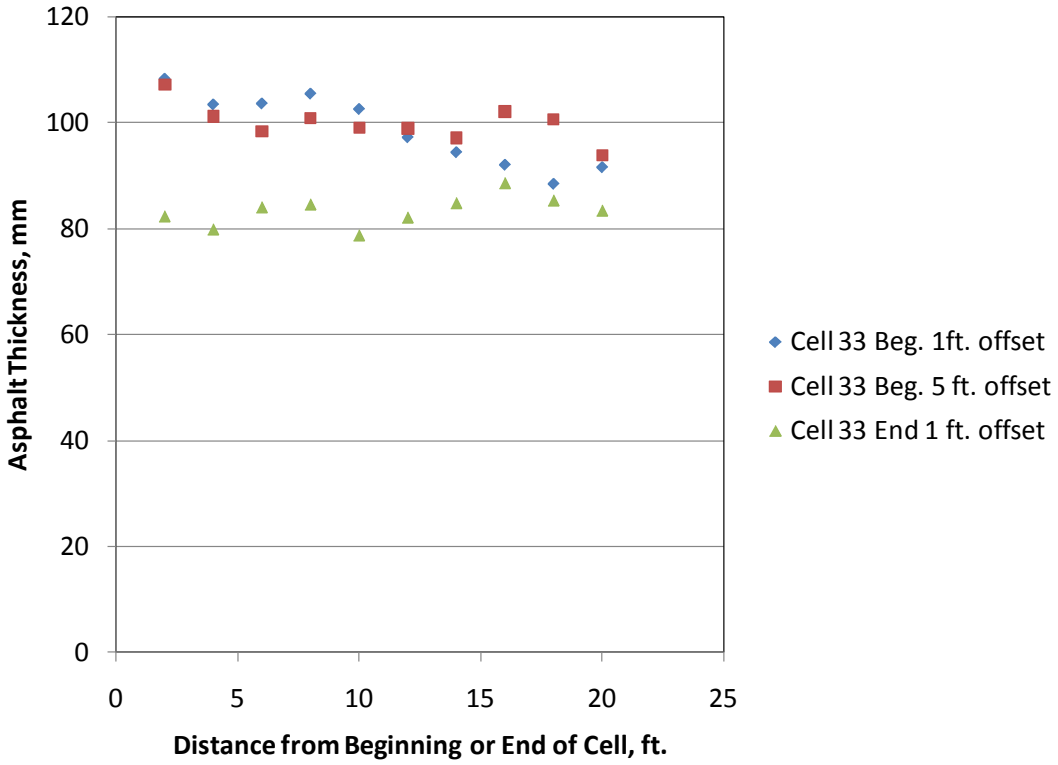

Figure B3. Cell 33 MIRA measured pavement thickness versus the distance from the start or end of the section

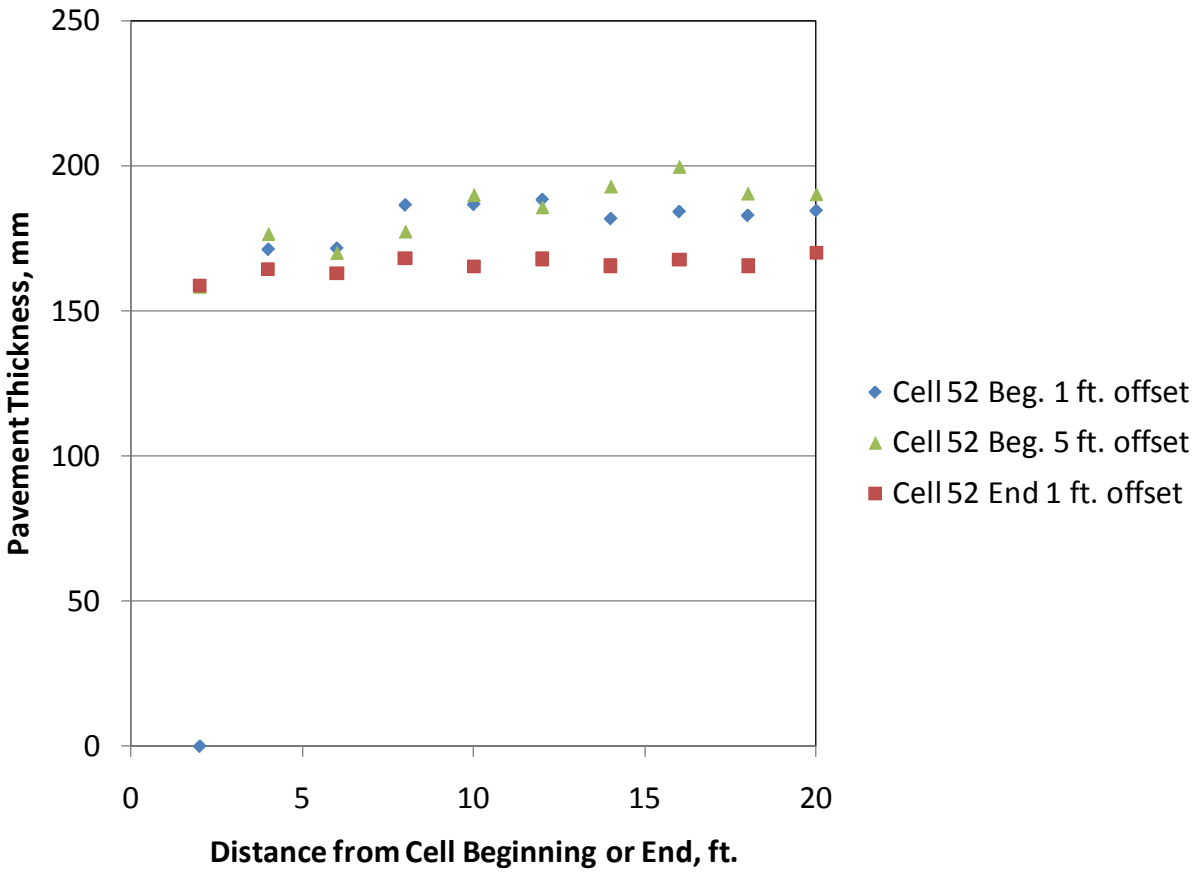

Figure B4. Cell 52 MIRA measured pavement thickness versus the distance from the start or end of the section

Figures B5 and B6 show the MIRA measured shear wave velocity versus measurement location for Cells 33 and 52, respectively. It can be observed from figure 5 that the Cell 33 shear velocity is lower in all measurement locations at 5 ft. from the paint strip versus 1 ft. from the paint strip. This should be expected, as the effective shear modulus should be higher due more compaction from traffic in the wheel path versus 5 ft from the paint strip where less wheel loads are applied. It can also be observed that the shear velocity is lower by a larger magnitude in all measurement locations at the end location of Cell 33. This drop in shear velocity is most likely due to the environmental conditions during testing. The beginning location Cell 33 scans were made in the morning when the asphalt pavement was drenched with rain water and an air temperature in the upper 30s Fahrenheit (see link 7). The end location Cell 33 scans where made after the pavement surface was almost dry after about 2 hours of no rain and an increased air temperature to about mid to high 40s Fahrenheit (link 8). The resulting increased asphalt binder temperature and corresponding lower shear modulus in the afternoon measurements most likely caused the lower shear velocity measurements at the end location of Cell 33. As can be observed from Figure B6, there didn't seem to be a significant difference in shear velocity in the PCC pavement section.

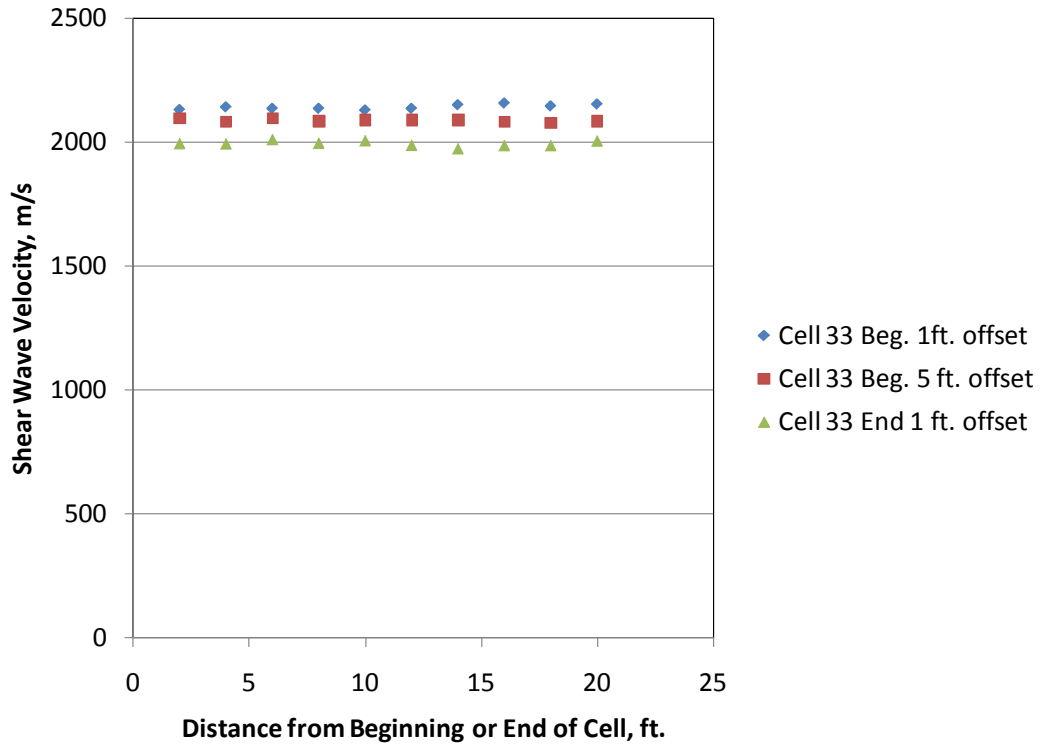

Figure B5. Cell 33 shear wave velocity vs. distance from start or end of section

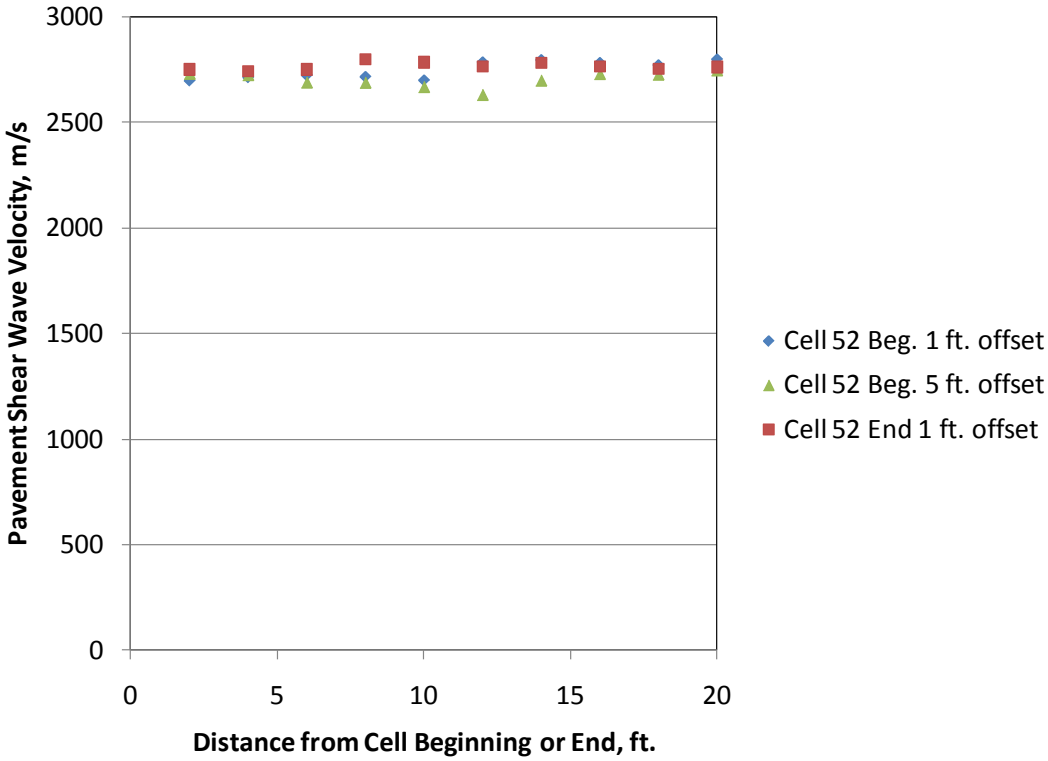

Figure B6. Cell 52 shear wave velocity vs. distance from start or end of section

Other Initial Observations

As briefly discussed in the results section, the asphalt binder temperature plays a significant role in the effective shear modulus and thus shear wave velocity. To quantify this effect, measurements were taken at Cell 33 in the afternoon in the same locations where measurements were taken in the morning. The measurements were taken directly after the end location Cell 33 measurements in the afternoon were taken with similar conditions as shown in link 9. Table B3 gives the values for both 1ft and 5 ft offsets and Figure B7 shows the decreasing trend in shear wave velocity between the morning measurements and the afternoon measurements for the 1 ft offset beginning of Cell 33 locations. It can be seen that while the relative trend from location to location is similar for both morning and afternoon measurements, the magnitude of the velocity is about 150 m/s lower on average in the afternoon. Figure B8 adds the non-wheel path data (5 ft offset) that was also taken in the morning to reference this effect to differences in compaction. It can be observed that the effect of asphalt binder temperature is more significant than wheel path versus non-wheel path even for a case of only an approximately 10 degree increase in temperature with cloud cover at a fairly mild climate.

Table B3. Shear velocities in the morning and afternoon at beginning locations, Cell 33

1 ft offset	**Measurement Location**	1	2	3	4	5	6	7	8	9	10
	Morning Velocity, m/s	2131	2142	2136	2136	2129	2136	2151	2158	2146	2154
	Afternoon Velocity, m/s	1986	1984	1974	1980	1967	1987	2009	2012	1992	1998
5 ft offset	**Measurement Location**	1	2	3	4	5	6	7	8	9	10
	Morning Velocity, m/s	2095	2082	2096	2085	2089	2089	2090	2081	2078	2085
	Afternoon Velocity, m/s	1938	1930	1943	1939	1935	1936	1937	1932	1930	1941

This has major implications for comparing air void content in asphalt pavement using MIRA. While it has been shown that evaluation of shear wave velocity can effectively differentiate between locations with relatively large variation in compaction even when the pavement is exposed to sun drenching (longitudinal joint versus non-longitudinal joint measurements last fall referenced in the previous quarterly report), the ability of shear velocity to evaluate small variation in compaction seems to be highly dependent on a uniform asphalt binder temperature for both measurement locations. In the fall testing referenced in the previous quarterly report, there was no observed difference in wheel path versus non-wheel path shear wave velocity, while the wheel path versus non-wheel path measurements taken in a more mild water drenched pavement showed a significant difference in this study. While it should be expected that sun-drenching will affect all areas fairly similarly, it seems that even a slight variation in how much sun one location gets compared to another changes the velocities enough to affect the air void comparison between the two locations. This is due to the small effect of compaction compared to temperature variation. Nevertheless, it seems that application of water drenching before

testing is promising as an effective procedural step in achieving the necessary uniformity in asphalt binder temperature for detailed air void comparisons.

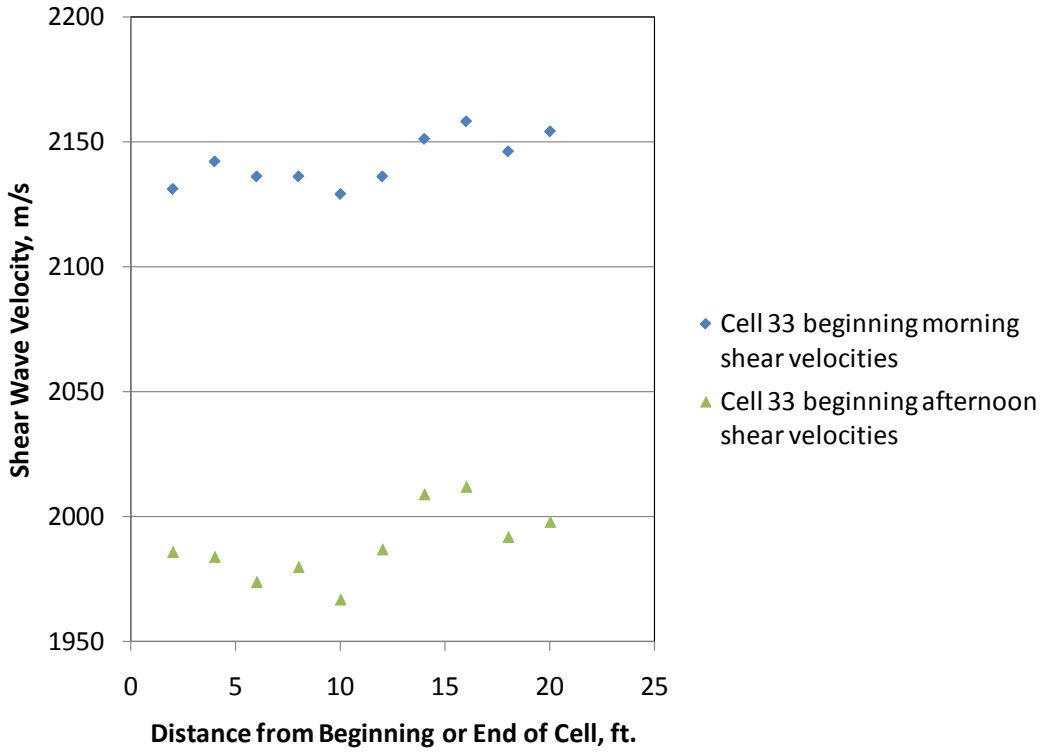

Figure B7. Beginning of Cell 33 1 ft. offset location shear velocities in the morning and afternoon

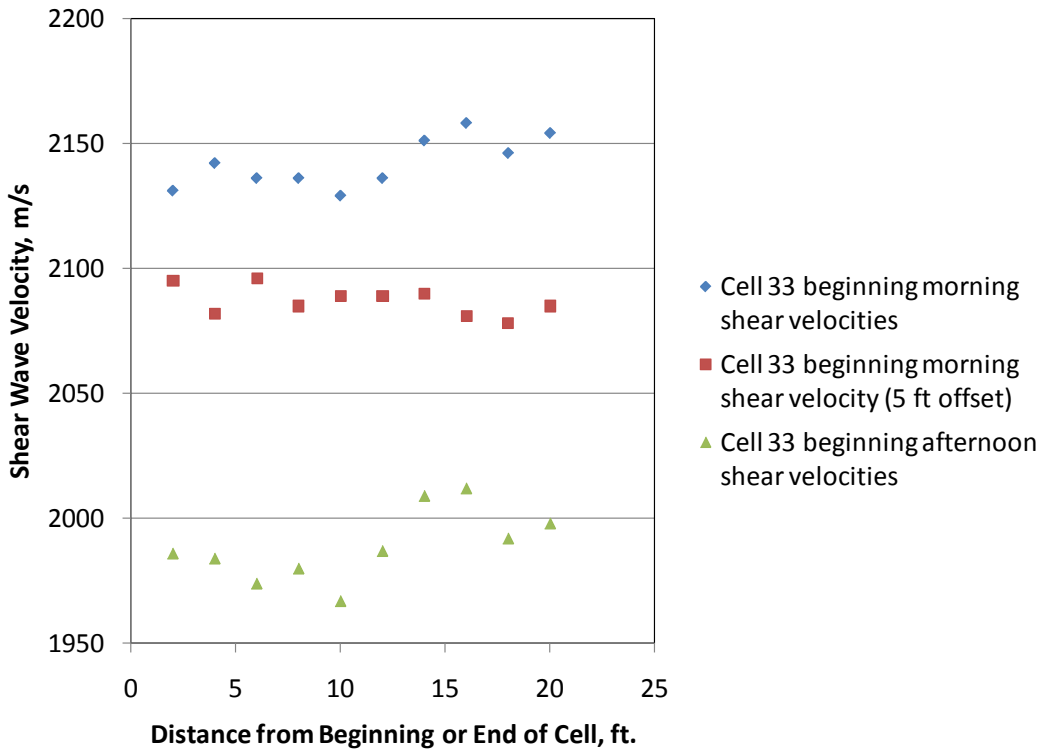

Figure B8. Beginning of Cell 33 1 ft. offset location shear velocities in the morning and afternoon with the addition of the beginning of Cell 33 5 ft. offset location shear velocities in the morning

In addition to the shear wave velocities collected in the afternoon at the same measurement locations at the beginning of Cell 33 that were taken in the morning, depth scans were also made. These scans have not been comprehensively analyzed yet, although an initial result at location 1 (108 mm MIRA measured thickness in the morning and 107 mm MIRA measured thickness in the afternoon) shows no significant difference in thickness measurement in the morning versus the afternoon.

Future Work

The depth scans discussed in the previous paragraph should be analyzed to verify if the increase in shear velocity in the afternoon affects the thickness measurements at the beginning of Cell 33. Analysis of these scans should also quantify the effect of a moderately increased binder temperature and surface drying on internal reflections and shadowing of the back wall reflection. In addition, analysis of the change in time between the backwall reflection from individual channel transmitting and receiving pairs located at variable distances should also be researched. This information can be used to calculate the shear wave velocity for comparison with the MIRA software calculated shear wave velocity and for possible correlation of this new calculated velocity with areas of different compaction. The effect of water drenching before testing should also be evaluated further.

There are also a few measurement locations where further information and/or forensic work would be beneficial. In one location (ID: Cell 52 – 1) a circular reflection approximately 85 to 90 mm depth is observed and shadowing of the backwall reflection inconsistent with a single circular scatterer of that size suggests the presence of some embedded atypical reinforcement, sensors and/or cables, or flaws. At the adjacent measurement location (ID: Cell 52 - 2) a similar circular reflection can be observed at a similar depth on the left hand side (-40 mm) of the MIRA aperture in addition to significant shadowing of the backwall reflection at on the left side of the aperture (away from the fog line). Contact with MnROAD employees has been initiated so that cores can be taken and information about the pavement Cell 52 design at that location and possible sensor information will be made available. The progression of scans and video documenting the scanning at these locations is shown on link 10.

Conclusions

Testing at MnROAD Cells 33 and 52 with the MIRA ultrasonic tomography device resulted in thickness and shear wave velocity measurements at 60 locations. GPR measurements taken at the same locations will allow for verification and research in how these two methods can complement each other in evaluating asphalt and PCC pavements. The results showed some variability in pavement thickness for Cells 33 and 52 as well as the effect of wheel path versus non-wheel path and environmental effects on shear wave velocity in asphalt pavement.

link 1: http://pavementndt.weebly.com/example-scanning-process.html
link2:http://pavementndt.weebly.com/measurement-location-requiring-additional scans.html
link 3: http://pavementndt.weebly.com/cell-33-table.html
link 4: http://pavementndt.weebly.com/cell-52-table.html
link 5: http://pavementndt.weebly.com/mnroad-cell-33-measurements.html
link 6: http://pavementndt.weebly.com/mnroad-cell-52-measurements.html
link 7: http://pavementndt.weebly.com/cell-33-morning-measurement-conditions.html
link 8: http://pavementndt.weebly.com/end-of-cell-33-afternoon-measurement-conditions.html
link 9: http://pavementndt.weebly.com/beginning-of-cell-33-afternoon-conditions.html
link 10: http://pavementndt.weebly.com/embedded-object-or-flaw-measurement-locations.html